INORGANIC CHEMISTRY FRONTIERS

RESEARCH ARTICLE

View Article Online
View Journal | View Issue



Cite this: *Inorg. Chem. Front.*, 2026, **13**, 637

# Phosphorus chirality assignment and solution dynamics of lanthanide(III) complexes of a monomethylphosphinate analogue of $H_4$dota: a multinuclear NMR and DFT study

Adam Svítok, [a] Carlos Platas-Iglesias, [b] Jan Kotek [a] and Petr Hermann *[a]

Analogues of $H_4$dota form kinetically inert and thermodynamically stable complexes with lanthanide(III) ions and they are used in many applications in biology and medicine, mostly as imaging or therapeutic agents. Many properties of the complexes depend on their solution isomerism and dynamics which, however, have not been so thoroughly studied for ligands with phosphinate-containing pendant arms. In particular, the absolute chirality of the phosphorus atom in the diastereoisomers detected in solution by NMR has not been assigned until now, and coordinated-noncoordinated oxygen atom exchange, a process analogous to the "phosphonate rotation" in phosphonate-containing derivatives, was not studied. Here, a model $H_4$dota analogue with one methylphosphinate group was prepared, and its $Ln^{III}$ complexes were studied by multinuclear ($^1$H, $^{13}$C, $^{17}$O, $^{31}$P) NMR and DFT calculations in solution and by X-ray diffraction in the solid state. Chiral pentavalent tetrahedral phosphorus atoms are present in a number of phosphorus acid derivatives. Here, we present the first method to determine the absolute *P*-chirality in solution using the paramagnetic relaxation enhancement (PRE) of $^{13}$C NMR signals of the $Yb^{III}$ complex. The method allowed the assignment of two major diastereoisomers of the complexes as *R*-Λλλλλ/*S*-Δδδδδ (*v*-TSA, *vertical* twisted-square antiprism) and *R*-Λδδδδ/*S*-Δλλλλ (*v*-SA, *vertical* square antiprism). The assignment agrees with the solid-state structure and DFT calculations. This method enables absolute *P*-chirality determination in $Ln^{III}$ complexes of various phosphorus acid $H_4$dota analogues in solution and can be also applied to other rigid systems. The "phosphinate rotation" process was observed by $^{17}$O/$^1$H–$^1$H EXSY NMR only for large $Ln^{III}$ ions and only in the TSA isomers. Its mechanism is analogous to that of the "phosphonate rotation" investigated recently on complexes of the mono(phosphonate monoester) $H_4$dota analogue, but the "phosphinate rotation" is more sterically demanding in complexes of smaller lanthanide(III) ions due to the higher bulkiness of the methyl group compared with the oxygen in the ester derivatives.

Received 11th September 2025,
Accepted 28th October 2025

DOI: 10.1039/d5qi01885d

rsc.li/frontiers-inorganic



## Introduction

Lanthanide(III) complexes of macrocyclic ligands derived from $H_4$dota (1,4,7,10-tetraazacyclododecane-1,4,7,10-tetraacetic acid, Fig. 1) are usually kinetically inert and thermodynamically stable. These properties efficiently decrease their *in vivo* toxicity, leading to many biological/medicinal applications. Thus, they are used as gadolinium(III)-based MRI contrast agents (MRI CA's),[1–6] carriers of metal radioisotopes for imaging and therapy,[5,7–9] fluorescence probes,[5,6,10–12] or as protein paramagnetic tags.[13–15] Over the years, investigations of various properties of $Ln^{III}$ complexes of this type of ligands have led to a better understanding of the chemistry and physics behind these applications.

The properties of these complexes, important for the applications mentioned above, depend on their solution isomerism. In the complexes, the $Ln^{III}$ ions are sandwiched between the $N_4$-plane formed by the cyclen nitrogen atoms and the $O_4$-plane defined by the oxygen atoms of the coordinating pendant arms.[16,17] This coordination leads to two diastereoisomers differing in the conformations of the macrocycle and pendant five-membered chelate rings. Thus, a combination of two possible macrocycle chelate ring configurations, δδδδ and λλλλ, and two possible pendant arms orientations, Δ and Λ, gives two diastereoisomers traditionally labelled as twisted-

[a]*Department of Inorganic Chemistry, Faculty of Science, Charles University, Hlavova 2030, 12843 Prague 2, Czech Republic. E-mail: petrh@natur.cuni.cz; Tel: +420-22195-1263*
[b]*Universidade da Coruña, Centro Interdisciplinar de Química e Bioloxía (CICA) and Departamento de Química, Facultade de Ciencias, 15071 A Coruña, Galicia, Spain*

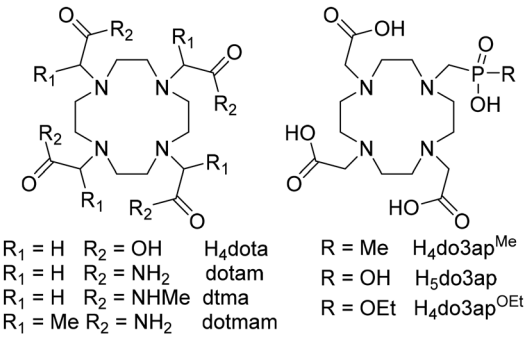


**Fig. 1** Structures of ligands discussed in the text.

square antiprism (TSA) and square antiprism (SA). Each diastereoisomer consists of an enantiomeric pair (ΔδδδδΛλλλλ for TSA and ΛδδδδΔλλλλ for SA). In addition, an apically coordinated water molecule may be present above the $O_4$-plane, leading to the coordination number nine (CN 9) for large $Ln^{III}$ ions. If the complexes are non-aquated (*i.e.*, having CN 8), the isomers are labelled as TSA′ and SA′, respectively. The abundance of the isomers in solution depends on $Ln^{III}$ size and ligand structure.[16,17] The TSA arrangement is preferred by large $Ln^{III}$ ions and bulky $H_4$dota derivatives as the ligand cavity in the TSA isomer is larger and more flexible than that of the SA isomer. In solution, the TSA/SA isomers are in a mutual dynamic exchange proceeding on a millisecond time scale.[16,18] The TSA/SA diastereoisomers interchange by inverting the macrocycle chelate ring conformations or by reorienting the pendant arms. A combination of both movements forms the other enantiomer of the diastereoisomer. Another dynamic process, an exchange between coordinated and non-coordinated carboxylate oxygen atoms of $H_4$dota, was observed by $^{17}O$ NMR, and it also happens on a millisecond time scale.[19–22] This "carboxylate rotation" exchanges the oxygen atoms without the SA/TSA interchange.

Carboxylate group(s) in $H_4$dota may be replaced with acidic moieties derived from phosphoric, phosphonic or phosphinic acid groups. Gradual substitution of carboxylates with bulkier phosphorus acid groups increases the TSA abundance in solution,[23–28] and $Ln^{III}$ complexes of tetraphosphorus acid $H_4$dota analogues occur only as the TSA isomers over the whole lanthanide series.[29–32] If an oxygen atom of a tetrahedral phosphinate or phosphonate monoester groups is coordinated to a metal ion, the phosphorus atom become chiral (*R*/*S*), leading to more diastereoisomers due to the combination of three chirality elements. Thus, $Ln^{III}$ complexes of $H_4$dota analogues with only one phosphinic acid/phosphonic monoester group have a maximum of four diastereoisomers (*i.e.* four enantiomeric pairs), *R*/*S*-SA and *R*/*S*-TSA. A full set of diastereoisomers is observed in complexes of $H_4$dota derivatives with phosphonate monoesters (having the P–OR bond) or phosphinates containing P–H/P-aryl bonds.[33–36] For compounds with P-alkyl bonds, one phosphorus atom configuration is highly preferred which lowers the number of the observed diastereoisomers; a single diastereoisomer is detected for complexes of tetraphosphinate $H_4$dota analogues.[31,32,35,36] Commonly, all isomers interchange but this isomerism in complexes of the phosphorus acid derivatives has not been studied in detail. Recently, we have studied these exchange processes on $Ln^{III}$ complexes of monophosphorus acid analogues of $H_4$dota, $H_5$do3ap and $H_4$do3ap$^{OEt}$ (Fig. 1), by multinuclear NMR spectroscopy and DFT calculations.[37,38] In the complexes of $H_5$do3ap, the pendant arm rotation (*i.e.*, the Λ/Δ exchange) was found to be faster than the macrocycle chelate ring inversion (*i.e.*, the λλλλ/δδδδ exchange), and the pendant arm movement was suggested to involve a transient bidentate $\kappa^2$-*O*,*O*′-$PO_2$ coordination of the phosphonate group.[38] This coordination mode was later confirmed in a transition state for the mutual exchange of coordinated/uncoordinated oxygen atoms of the chiral phosphonate monoester group ("phosphonate rotation") of $H_4$do3ap$^{OEt}$ by multinuclear ($^1H$, $^{17}O$ and $^{31}P$) NMR investigations and DFT calculations.[37] However, the absolute *R*/*S* configuration of the phosphorus atom in individual diastereoisomers could not be determined.

As mentioned above, one *P*-configuration is preferred in the complexes of phosphinate $H_4$dota analogues with P-alkyl substituents.[25,27,31,32,35,36] However, there has been no method suggested for determination of the absolute *P*-configuration of the diastereoisomer until now. Moreover, labelling the phosphinate group with $^{17}O$ in a monophosphinate $H_4$dota derivative offers a possibility to investigate the dynamics of the complexes analogously to the mono(phosphonate monoester) ligand.

Different pentavalent phosphorus acid derivatives (phosphoric acid esters, sulfur or nitrogen derivatives *etc.*) can also contain a chiral tetrahedral phosphorus atom. These compounds are inherently chiral or become chiral after their coordination to a metal ion (*e.g.* in an enzyme active site) if they contain the $(>PO_2)^-$ fragment. They are present in nature and their biological behaviour (*e.g.* ester hydrolysis) often depends on the phosphorus atom chirality.[39–42] However, a direct experimental determination of their absolute *P*-configuration in solution is problematic.

In this work, we present a new method for the determination of the absolute configuration of the coordinated phosphorus atom in compounds with a tetrahedral phosphoryl group. Thus, we prepared the $^{17}O$-labelled mono(methylphosphinic acid) derivative $H_4$do3ap$^{Me}$ (Fig. 1) and its $Ln^{III}$ complexes, and we investigated the complexes by multinuclear NMR and DFT calculations. Activation parameters for the coordinated/non-coordinated oxygen atoms exchange of the $(>PO_2)^-$ group, "phosphinate rotation", were determined for the $H_4$do3ap$^{Me}$ complexes and compared with those of the "phosphonate rotation" in the $H_4$do3ap$^{OEt}$ complexes. Identifying the preferential orientation of the phosphorus atom substituent(s) in the complexes can be useful to fine tuning the physico-chemical properties of the macrocyclic complexes. Furthermore, the $(\kappa^2$-$PO_2)^-$ coordination mode of the tetrahedral oxophosphorus groups, involved in the isomer interconversion, has been only sparingly experimentally or theoretically investigated.[43–46] Thus, the data presented here

 

also contribute to a fundamental understanding of the coordination behaviour of the tetrahedral phosphorus acid anions.

For clarity reasons, in the following text and in the SI, the coordinated water molecule is omitted in all formulae, labels and pictures, and the complexes are denoted with general formulae $[Ln(ligand)]^{n-}$.

## Results and discussion

### Synthesis of ligands and complexes

The non-labelled ligand $H_4do3ap^{Me}$ was prepared by a phospha–Mannich reaction of a macrocyclic precursor, $t$Bu$_3$do3a·HBr, with isopropyl methyl-*H*-phosphinate in anhydrous pyridine, catalysed by one equivalent of HBr. This procedure avoids the use of oxidation-prone free methyl-*H*-phosphinic acid in the Moedritzer–Irani variant[47] of the phospha–Mannich reaction in aqueous HCl. Next, the esters were hydrolysed to afford $H_4do3ap^{Me}$ in an overall 73% isolated yield (based on $t$Bu$_3$do3a·HBr). It should be mentioned that the use of methyl or ethyl esters of methyl-*H*-phosphinic acid in the reaction led to significantly lower yields due to the competing reductive *N*-methylation of $t$Bu$_3$do3a (coupled with the P–H bond oxidation) and phosphinic ester hydrolysis (see also below). The $^{17}$O-enriched $H_4do3ap^{Me}$ was prepared (Scheme 1) by a multi-step synthesis incorporating $^{17}$O in the first step, as the phosphinate group cannot be enriched by heating with $H_2{}^{17}O$ in acidic solutions, unlike the carboxylate group.[48] Methyl-dichlorophosphine was hydrolysed by $^{17}$O-enriched water (approx. 12% $^{17}$O) to get the $^{17}$O-enriched methyl-*H*-phosphinic acid. To preserve the $^{17}$O isotope in the structure, the acid was esterified by an alkylation with $(Et_3O)BF_4$ in the presence of 2,6-lutidine as a weak base to prevent an alkylation of the phosphorus atom.[49] The $^{17}$O-enriched ethyl methyl-*H*-phosphinate reacted with the macrocyclic precursor, $t$Bu$_3$do3a·HBr, similarly to the non-labelled compound. Finally, the phosphorus ester groups were removed by TMS-Br, preserving the $^{17}$O-labelling,[50] and the $t$Bu groups were cleaved by anhydrous TFA. The overall isolated yield of the $^{17}$O-labelled $H_4do3ap^{Me}$ was 17% (four steps; based on $MePCl_2$). The low yield can be attributed to the low stability of the required $^{17}$O-labelled ethyl *H*-phosphinate precursor, which is caused mainly by oxidation of the P–H bond (connected with reductive *N*-methylation of $t$Bu$_3$do3a) and decomposition (ester hydrolysis) of the labelled ethyl methyl-*H*-phosphinate (see above). Lanthanide(III) complexes of $H_4do3ap^{Me}$ (both labelled and non-labelled) were prepared by reacting $LnCl_3$ with a slight ligand excess in aqueous solutions to ensure that free $Ln^{III}$ ions were fully complexed in the final mixture. Solid-state structures of the unlabelled $H_4do3ap^{Me}$ ligand and the $[Yb(do3ap^{Me})]^-$ complex were determined by X-ray diffraction and are discussed in SI and below (Fig. 5 and S1, S2).

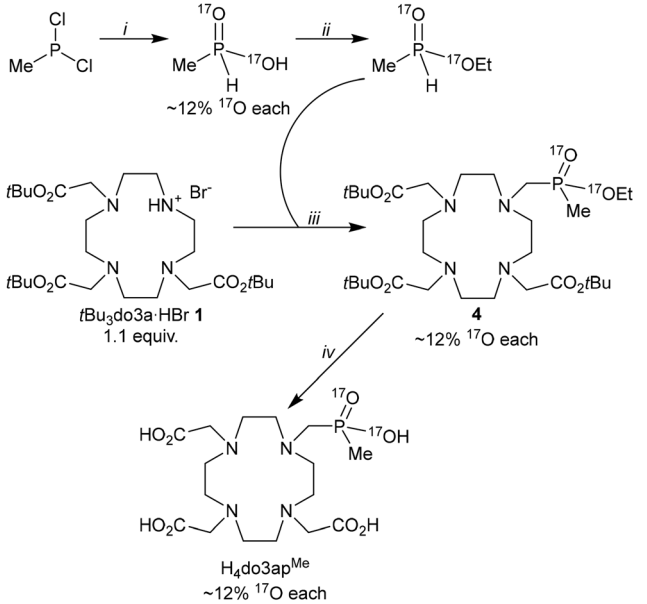


**Scheme 1** Synthesis of $^{17}$O-enriched $H_4do3ap^{Me}$: (i) $H_2{}^{17}O$ (12% $^{17}$O, 2.5 equiv.), anhydrous THF, 0 °C → room temperature (r.t.), 12 h; (ii) $[Et_3O][BF_4]$ (2.6 equiv.), 2,6-lutidine (2 equiv.), anhydrous $CH_2Cl_2$, 0 °C → r.t., 3 h; (iii) paraformaldehyde (4 equiv.), $CH_2Cl_2$/pyridine (1 : 2), 40 °C, 36 h; (iv) 1. TMSBr (12 equiv.), anhydrous $CHCl_3$, r.t., 72 h; 2. $CH_3OH$, r.t., 1 h; 3. $CH_2Cl_2$/TFA (1 : 1), r.t., 2 d.

### Phosphorus atom absolute configuration and diastereoisomer assignment

The $[Ln(do3ap^{Me})]^-$ complexes form up to four diastereoisomers, each consisting of an enantiomeric pair, by a combination of the macrocycle chelate ring conformations δδδδ/λλλλ, the pendant arms orientations Δ/Λ (leading to the SA or TSA arrangements), and *R*/*S* configurations on the phosphorus atom of coordinated phosphinic group (Fig. 2). Here for the first time, it was possible to assign the absolute orientation of the phosphorus atom substituents and to distinguish the phosphorus-based isomers. In the following text, we will use abbreviations "*v*-TSA/*v*-SA" and "*h*-TSA/*h*-SA" where "*v*" and "*h*" denote "*vertical*" and "*horizontal*" positions of the *P*-substituents, respectively. In the "*vertical*" isomer, the phosphorus substituent is directed approximately perpendicularly to the $O_4$ plane of the complex. In the "*horizontal*" isomer, the phosphorus substituent lies approximately horizontally to the $O_4$ plane of the complex. Here, all four diastereoisomers could be detected by NMR but signals of two minor diastereoisomers were often unidentifiable due to a low signal intensity as a result of the low abundance of the isomers (Fig. S4–S9).

In previous works on $Ln^{III}$ complexes of cyclen–phosphinate derivatives,[25,27,31,32,35,36,51,52] their TSA/SA geometry in solution was easily assigned by their $^1$H NMR spectra. However, it was impossible to determine the orientation of the phosphorus atom substituent (*i.e.*, the *R*/*S* configuration). For a better interpretation of experimental and computational data here (see below), it is advantageous to assign the *R*/*S* configuration on the phosphorus atom in each diastereoisomer of the $[Ln(do3ap^{Me})]^-$ complexes. Thus, we analysed the lanthanide-induced paramagnetic relaxation enhancement (PRE) effect on the $^{13}$C NMR signals to determine experimentally the

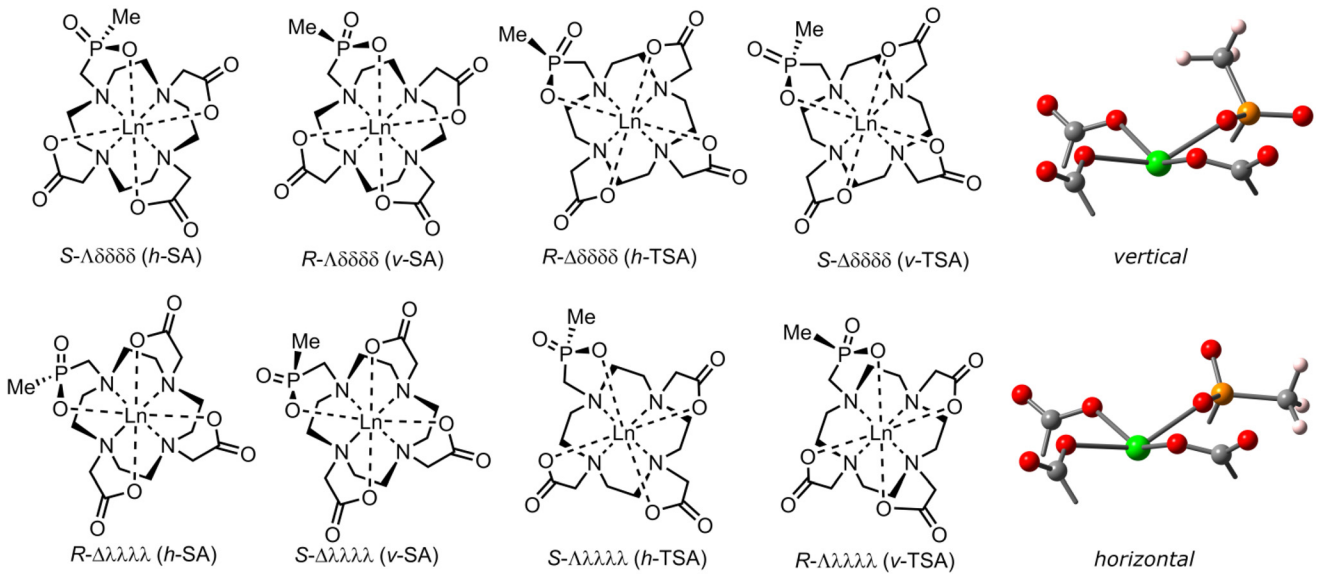


**Fig. 2** Schematic representation of all possible isomers of [Ln(do3ap$^{Me}$)]$^{-}$ complexes; charges and the coordinated water molecule are omitted. The upper row shows four diastereoisomers with their enantiomeric pair placed right below. The coloured structures (right) show orientation of the *P*-bound methyl group in relation to the $O_4$ plane in the *vertical* (*v*-) and the *horizontal* (*h*-) isomers.

*P*-substituent orientation in the different diastereoisomers. For the experiment, the [Yb(do3ap$^{Me}$)]$^{-}$ complex was selected due to the abundance of only one major diastereoisomer (either *h*-TSA′, or *v*-TSA′), its slow dynamics and the knowledge of its solid-state structure (see below). Theoretically, complexes of any paramagnetic Ln$^{III}$ might be used but those with a larger PRE are preferred. Here, the Yb$^{III}$ complex was selected due to the difficulty of assigning NMR signals in complexes of Ln$^{III}$ ions with larger PRE (for details, see Experimental part).

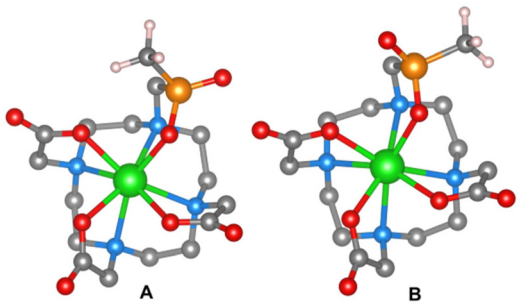


**Fig. 3** The DFT-calculated structures of the *v*-TSA′ (A) and *h*-TSA′ (B) diastereoisomers of [Yb(do3ap$^{Me}$)]$^{-}$; colour code: carbon – grey, hydrogen – white, nitrogen – blue, oxygen – red, phosphorus – orange and ytterbium – green. Hydrogen atoms, except those at the methyl group, are omitted for clarity. Visualised in VESTA software.[53]

Structures of the diastereoisomers were calculated by DFT and are shown in Fig. 3. The distances between the methyl carbon atom and the Yb$^{III}$ ion, determined by the DFT calculations, differ significantly between the *h*-TSA′ and *v*-TSA′ diastereoisomers (4.75 *vs.* 4.40 Å, respectively) and, thus, can be used to unambiguously assign the diastereoisomers. The distances determined from the $^{13}$C NMR relaxation times (Table S3), by DFT calculations and by X-ray diffraction are given in Table 1. The $^{13}$C PRE method was first tested by determination of the distances between Yb$^{III}$ ion and the easily assignable (Fig. S10 and the accompanying text) carboxylate $^{13}$C atoms. The distances found in the solid state, determined by DFT calculations and by the PRE method, are all in good agreement. Then, the same comparison was done for the *P*-bound methyl carbon atom; its $^{13}$C NMR signal was assigned by a selective $^{1}$H decoupling (Fig. S11). The experimental $H_3\underline{C}\cdots$Yb distance determined by $^{13}$C PRE is close to that found/calculated for the *R*-Λλλλλ/*S*-Δδδδδ, *vertical*-TSA (*v*-TSA), diastereoisomer (Fig. 3).

Previously, this method was used to determine the Tb/Dy/Ho···H distances in $H_4$dota complexes.[54] A similar

**Table 1** The Yb···C distances (Å) determined by X-ray diffraction, DFT or PRE for the *v*-TSA′/*h*-TSA′ diastereoisomers of the [Yb(do3ap$^{Me}$)]$^{-}$ complex

| | Distances, Å | | | |
|---|---|---|---|---|
| Isomer/method | $d_1$(OC···Yb) | $d_2$(OC···Yb) | $d_3$(OC···Yb) | $r$($H_3$C···Yb) |
| *R*-Λλλλλ/*S*-Δδδδδ *v*-TSA′ (X-ray) | 3.17 | 3.13 | 3.09 | 4.31 |
| *R*-Λλλλλ/*S*-Δδδδδ *v*-TSA′ (DFT) | 3.15 | 3.14 | 3.13 | 4.40 |
| *S*-Λλλλλ/*R*-Δδδδδ *h*-TSA′ (DFT) | 3.15 | 3.14 | 3.13 | 4.73 |
| PRE | 3.1 | 3.0 | 3.0 | 4.2 |

method has been also used to determine the Ln···X distances. The Tb/Nd/Sm···H distances were determined in complexes of various ligands by comparing the paramagnetic relaxation times of different $^{1}$H atoms[55–57] (see below) and Tb/Dy/Ho/Er/Tm/Yb···F/P distances were determined from paramagnetic $T_{1,M}$ relaxation times determined at multiple magnetic fields.[58,59] Moreover, Gd···Y/C distances were obtained using only the $T_{1,M}$ of $^{89}$Y shortened by Gd$^{III}$, which is possible due to the magnetic properties of the Gd$^{III}$ ion.[60]

The PRE method has some advantages and limitations. It might be generally applied to determine Ln···X distances in compounds where "X" is a non-quadrupolar NMR-active nucleus and various paramagnetic lanthanide(III) ions can be used. The complex or system should be (semi)rigid on NMR time scale. In chemistry of macrocyclic complexes, the method may be used to define diastereoisomers, to assign NMR signals or to determine the solution structure. In biochemistry, it could be used if the compound of interest is locked (*e.g.* inside a peptide) and the paramagnetic probe is bound at such a distance that PRE of the "X" nucleus is measurable. The main advantage of using lanthanide-induced relaxation is its independence on the position/orientation of the magnetic axis of the complex, unlike lanthanide-induced shifts (LIS).[61]

The method utilizing the difference between relaxation rates $R_2$ and $R_1$, presented here, could be used for these purposes with the advantage of not requiring multiple magnetic fields, the knowledge of some Ln···X distance or a large distance from the Ln$^{III}$ ion in the case of Gd$^{III}$. However, it requires determination of the $T_2$ relaxation time and the rotational correlation time $\tau_R$. Nowadays, the method may be used in the rapidly growing field of $^{19}$F MRI, where the Ln···$^{19}$F distance is one of the most important parameters of potential contrast agents. Due to the long $T_1$ relaxation times of $^{19}$F, paramagnetic relaxation enhancement of $^{19}$F is advantageous and complexes of various Ln$^{III}$ are studied for this purpose. Both $T_1$ and $T_2$ of $^{19}$F MRI in these contrast agents strongly depend on the Ln···$^{19}$F distance which affects the $^{19}$F MRI signal intensity and contrast.

The $H_3\underline{C}$···Yb distance can also be determined from the ratio of paramagnetically enhanced $R_{1M}$ relaxation rates of the carbonyl and methyl carbon atoms (Table S3). Average values of $d(H_3\underline{C}\cdots Yb)$ = 4.40 and 4.45 Å were determined at 0 °C and 5 °C, respectively, assigning the shorter distances to the faster relaxation rates. These values agree well with the $H_3\underline{C}$···Yb distance in the *vertical* *R*-Λλλλλ/*S*-Δδδδδ (*v*-TSA) diastereoisomer (Table 1).

The *R*-Λλλλλ/*S*-Δδδδδ (*v*-TSA) isomer is also energetically favoured by DFT calculations, being ~4 kJ mol$^{-1}$ lower in energy at 25 °C (Table S4) over the entire Ln$^{III}$ series. Based on $^{1}$H and $^{31}$P NMR spectra (Fig. S4–S6), the major diastereoisomers have the same phosphorus configuration for all [Ln(do3ap$^{Me}$)]$^-$ complexes. The *h*/*v*-SA diastereoisomers were assigned based on $^{1}$H–$^{1}$H EXSY of the Eu$^{III}$ complex which distinguishes macrocycle inversion from pendant arms re-orientation. The major *v*-TSA diastereoisomer interchanges with the major SA diastereoisomer by macrocycle inversion (see Fig. 6 below). Thus, the major SA diastereoisomer must be the *vertical*-SA (*v*-SA). Based on DFT, the *v*-SA is also the energetically favoured SA diastereoisomer for all complexes (Table S4).

By comparing the relative $^{1}$H chemical shifts with those of the [Ln(do3ap$^{OEt}$)]$^-$ complexes studied previously (Fig. 4),[37] the major SA diastereoisomer is the same, *vertical*-SA (*v*-SA), as for the title phosphinate complexes but the major TSA diastereoisomer is the other one: *horizontal*-TSA (*h*-TSA). This correlates with $^{1}$H–$^{1}$H EXSY data, which showed that the major TSA and SA diastereoisomers of the $H_4$do3ap$^{OEt}$ complexes interchange by pendant arms re-orientation,[37] unlike the major diastereoisomers of [Ln(do3ap$^{Me}$)]$^-$. Thus, if the major SA isomer of [Ln(do3ap$^{OEt}$)]$^-$ is the *v*-SA, the major TSA diastereoisomer of [Ln(do3ap$^{OEt}$)]$^-$ must be the *h*-TSA.[37]

For the [Ln(do3ap$^{Me}$)]$^-$ complexes, abundances of the SA/TSA diastereoisomers were determined from relative intensities (as the sum of the *v*-SA + *h*-SA and *v*-TSA/*v*-TSA′ + *h*-TSA/*h*-TSA′ signal integrals, respectively) of their $^{1}$H and $^{31}$P NMR signals at 5 °C (Fig. S13). The abundances depend on the Ln$^{III}$ size similarly to complexes of other $H_4$dota derivatives – SA abundance increases with decreasing Ln$^{III}$ size to Dy$^{III}$ and then decreases after this Ln$^{III}$ ion. The trend originates from a smaller ligand cavity of the SA isomers *vs.* TSA isomers and from an even smaller ligand cavity of the TSA′ isomers, better accommodating the smallest Ln$^{III}$ ions.[24,62] Energies determined by DFT also follow this trend (Table S4). Analogously to the [Ln(do3ap$^{OEt}$)]$^-$ complexes, the abundances of the TSA diastereoisomers increase with a higher temperature but ratios of the *vertical*/*horizontal* diastereoisomers remain nearly constant for all *v*/*h*-TSA, *v*/*h*-SA and *v*/*h*-TSA′ pairs at all measured temperatures (Fig. S13 and Table S5). Moreover, the relative ratios of *vertical*/*horizontal* diastereoisomers are independent of Ln$^{III}$ ions, and they are approximately 96%, 90% and 95% for *v*-SA : *h*-SA, *v*-TSA : *h*-TSA and *v*-TSA′ : *h*-TSA′ ratios, respectively (Table S6). Based on DFT, these ratios slightly vary, but the calculated energy differences are negligible, especially when compared with calculated differences in the TSA/SA ratio (Fig. S4). For the [Ln(do3ap$^{OEt}$)]$^-$ complexes, these ratios are also independent of Ln$^{III}$ and temperature but the mixtures contain only approximately 65% of the major diastereoisomer (*v*-SA, *h*-TSA or *h*-TSA′) for all of *v*-SA : *h*-SA, *h*-TSA : *v*-TSA and *h*-TSA′ : *v*-TSA′ ratios.[37] Accordingly, energy differences of dia-

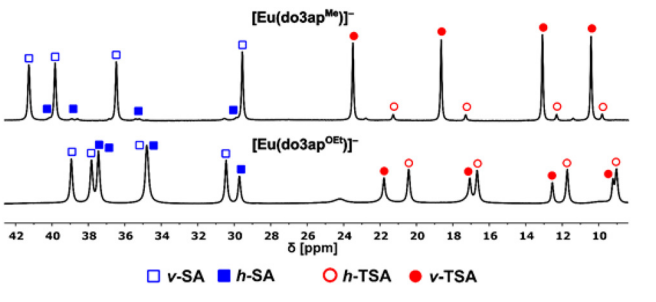


**Fig. 4** A comparison of $^{1}$H NMR spectra of the axial protons of [Eu(do3ap$^{Me}$)]$^-$ (top) and [Eu(do3ap$^{OEt}$)]$^-$ (bottom, data from ref. 37) complexes at 5 °C and $\nu$($^{1}$H) = 600 MHz.

stereoisomers in these pairs calculated by DFT are minimal for $[Ln(do3ap^{OEt})]^-$ and do not even allow for predicting the more stable phosphorus configuration (Fig. S4). Thus, the character and abundance of major diastereoisomeric species in solution differ for various phosphorus substituents. This agrees with previous studies of solutions of complexes of tetraphosphorus $H_4$dota derivatives (see below).

To gain more insight on the influence which the nature of *P*-substituent has on the relative energy of the isomers, we carried out additional DFT calculations on $[Eu(do3ap^R)]^-$ complexes, where R = H (the smallest substituent, a full isomer set is generally observed in solution) or the unknown analogue with R = *t*Bu (a bulky substituent; a preference for the *vertical* isomer is expected). The relative energies of the isomers in this series of phosphorylated derivatives (R = H, OEt, Me and *t*Bu) were subsequently compared. If the *P*-bound atom/group is small (R = H or OEt), the energy differences between the *vertical* and *horizontal* isomers are small (~1 kJ $mol^{-1}$), with the lowest-energy isomers being the *horizontal* ones. For bulkier groups (R = Me or *t*Bu), the differences were more significant (~3–8 kJ $mol^{-1}$) and these differences were more pronounced for the bulky *t*Bu group. The *vertical* isomers were strongly preferred for the latter complexes, indicating that steric requirements probably impose the isomer preferences.

## Solid-state structures

The solid-state structures of the $[Yb(do3ap^{Me})]^-$ and $[Yb(do3ap^{OEt})]^-$ complexes (Fig. 5) were studied to determine the phosphorus atom configuration and compare the structures with the solution data (Fig. S3 and Table S1). The solid-state structure of $[Li(H_2O)_3][Yb(do3ap^{Me})]\cdot H_2O$ contains two complex enantiomers *R*-Λλλλλ and *S*-Δδδδδ corresponding with the *v*-TSA′ isomer while the $[Li(H_2O)_3][Yb(do3ap^{OEt})]\cdot H_2O$ structure contains the two enantiomers *S*-Λλλλλ and *R*-Δδδδδ corresponding with the *h*-TSA′ isomer, analogously to the *h*-TSA′ isomers of the $[Ho/Er(do3ap^{OEt})]^-$ anions found in the solid state previously.[37] The *trans*-O-Yb-O opening angles of 119.7° and 130.1° for $[Yb(do3ap^{Me})]^-$, and of 121.5° and 129.4° for $[Yb(do3ap^{OEt})]^-$ are lower than the limiting value of ~135° for the TSA isomers to accommodate a coordinated water molecule.[24,63,64] Thus, the structures are better labelled as v/*h*-TSA′, which is further supported by the twist angles between the $O_4$ and $N_4$ planes of 26.2–27.4° and 27.6–28.9° for $[Yb(do3ap^{Me/OEt})]^-$, respectively.[24,63,64] The *v*-TSA′ and *h*-TSA′ diastereoisomers found for the $[Yb(do3ap^{Me/OEt})]^-$ complexes, respectively, correspond to the major diastereoisomers observed in solutions of these complexes (see above) and with the major diastereoisomers predicted by DFT (Table S4).

The solid-state structures of complexes of $H_4$dota derivatives with one (4-nitro-benzyl)- or (dibenzylamino)methylphosphinate pendant arm also contain only the *v*-TSA isomer.[27,64,65] In solution, $Ln^{III}$ complexes of these and all other monophosphinic acid $H_4$dota analogues ($DO3AP^R$ ligands) have only one major TSA diastereoisomer (>95%), similarly to the title $[Ln(do3ap^{Me})]^-$ complex.[25,27,60,66] Complexes of tetra(alkylphosphinic acid) $H_4$dota analogues ($DOTP^R$ ligands, R = Me, Et, Bn, $CH_2OH$ *etc.*) were found in the solid state also exclusively as the *v*-TSA isomers[31,32] and only one major TSA diastereoisomer was observed for their complexes in solution.[31,32,35,36,51,67] On the other hand, complexes of ligands with phenyl–phosphinate, *H*-phosphinate or phosphonate monoester pendants contain the *h*-TSA species[33,35,37,68] or a mixture of *v*-TSA and *h*-TSA isomers[35] in their solid-state structures. Similarly to the $[Ln(do3ap^{OEt})]^-$ complexes,[26,37] solutions of complexes of these ligands always contain a mixture of all possible diastereoisomers, *i.e.*, four *h*/*v*-SA and *h*/*v*-TSA isomers. For complexes of these tetraphosphorus acid derivatives, mixtures of diastereoisomers have been observed (up to eight isomers; they are only present as TSA species).[33–36]

Comparison of the solid-state structures with the solution isomer speciation allows a general assessment of about the influence of the *P*-substituents in phosphorus acid pendant arms of polyaza-macrocyclic ligands on the stereochemistry of their complexes. Preferential orientation of the phosphorus atom substituents and, thus, abundances of diastereoisomers of the complexes depend on the substituents, and two types of substituents can be distinguished. (i) Phosphinate groups with *P*-alkyl substituents form predominantly complexes with the "*vertical*" orientation of the substituent(s) in both TSA/SA species. This leads to two major diastereoisomers (in sum >95%), *v*-TSA and *v*-SA, for the $Ln^{III}$ complexes of $DO3AP^R$ derivatives and to one major (>90%) *v*-TSA diastereoisomer for complexes of $DOTP^R$ derivatives, as all phosphorus atoms have the same configuration. (ii) Phosphonate monoester groups, or phosphinates substituted with a phenyl group or with a P–H bond (R = OR′, aryl, H) form complexes which are present in solution as a mixture of (all) possible diastereoisomers. Complexes of these $DO3AP^R$ derivatives exhibit two major diastereoisomers (approx. 60–70%) in solution. The relatively low excess of the major isomers agrees well with DFT calculations (Table S4) as relative energy differences between all isomeric complexes of $H_4do3ap^{OEt}$ are smaller than relative energy differences between isomers of $H_4do3ap^{Me}$ complexes. Based on the data above and those in the literature, we can state that major isomers of complexes of these $DO3AP^R$ derivatives

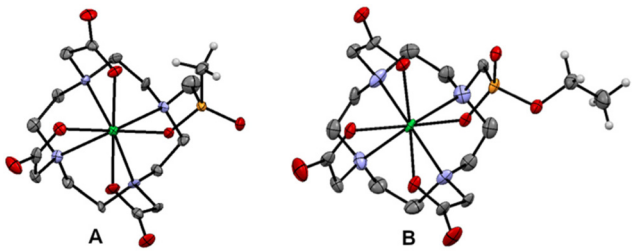


**Fig. 5** Molecular structures of $[Yb(do3ap^{Me})]^-$ (*v*-TSA′ isomer, A) and $[Yb(do3ap^{OEt})]^-$ (*h*-TSA′ isomer, B) anions found in the solid state. Macrocycle and pendant arm hydrogen atoms are omitted. Colour codes: carbon – grey, hydrogen – white, nitrogen – blue, oxygen – red, phosphorus – orange and ytterbium – green; numbering scheme is given in SI (Fig. S3).

should have the *h*-TSA and *v*-SA arrangements. For complexes of DOTP$^{R}$ ligands with these *P*-substituents (forming only the TSA isomers), up to all eight possible phosphorus-based diastereoisomers have been observed in solution. In both categories, preference for the phosphorus atom configuration does not depend on the size of Ln$^{III}$ ions (see also above).

The configuration on the coordinated phosphorus acid groups induced by the character of the *P*-substituents can also be extended to complexes of other trivalent metal ions with tris-phosphorus acid analogues of $H_3$nota; these hexacoordinated complexes exhibit stereochemistry analogous to the SA/TSA isomerism of $H_4$dota complexes and contain chiral phosphorus atoms. In the solid state, they have an SA-like combination of ring- and pendant arm-based chiralities ($\Delta\lambda\lambda\lambda/\Lambda\delta\delta\delta$). The solid-state structures of Fe$^{III}$, Co$^{III}$, Ga$^{III}$ and In$^{III}$ complexes with tris(phenyl-phosphinic acid) analogue of $H_3$nota have three *vertical P*-substituents, in agreement with the preferences given above for the SA isomers.[69] Similarly, the Ga$^{III}$ complex of the ligand with R = $CH_2CH_2CO_2H$ has three *vertical P*-substituents in the solid state.[70] However, in solution, gallium(III) complexes of tris(R-phosphinic acid) $H_3$nota analogues with R = $CH_2CH_2CO_2H$ or $CH_2OH$ are present as one major (>90%) isomer but the complex of the ligand with R = H has at least four diastereoisomers.[70,71] Thus, phosphorus stereochemistry in complexes of macrocyclic ligands controlled by the *P*-substituents seems to be a general phenomenon and might be used for a prediction of the phosphorus-based stereochemistry in systems where a detailed analysis suggested here cannot be carried out.

## Dynamic processes

Dynamic processes were investigated on the [Eu(do3ap$^{Me}$)]$^-$ complex whose EXSY spectra are measurable and evaluable due to the relatively low PRE of the Eu$^{III}$ ion. Signals of the axial (ax) protons (for their definition, see SI in ref. 37) were assigned by analogy with the [Eu(dota)]$^-$ and [Eu(do3ap)]$^{2-}$ complexes.[38,72] Signals of the equatorial (eq) protons were assigned by 2D $^1$H–$^1$H EXSY (Fig. S15) and $^1$H–$^1$H COSY (Fig. S16) experiments. In the 2D $^1$H–$^1$H EXSY spectrum, cross-peaks relating the axial and equatorial protons of *v*-TSA/*v*-SA and *h*-TSA/*h*-SA pairs confirm the interchange by the macrocycle inversion. Cross-peaks of both axial or both equatorial protons of *h*-TSA/*h*-SA and *v*-TSA/*v*-SA pairs confirm exchange by the pendant arms re-orientation. Moreover, detected cross-peaks of *h*-TSA/*v*-TSA exchange correspond to a phosphinate rotation. Similarly to the phosphonate rotation in the [Eu(do3ap$^{OEt}$)]$^-$ complex,[37] a phosphinate rotation interconverting *h*-SA/*v*-SA was not detected, as seen from the absence of cross-peaks of the axial *h*-SA/*v*-SA protons (Fig. 6).

Next, rates of the dynamic processes were determined using 2D $^{31}$P–$^{31}$P EXSY spectra (Fig. S17) as the signals of the isomers overlap in 2D $^1$H–$^1$H EXSY spectra. The 1D $^1$H EXSY spectra applied for this purpose previously[37,38] could not be used here due to the low signal intensities of the minor diastereoisomers. The rate constants for all processes were calculated from integral intensities of the cross- and diagonal peaks

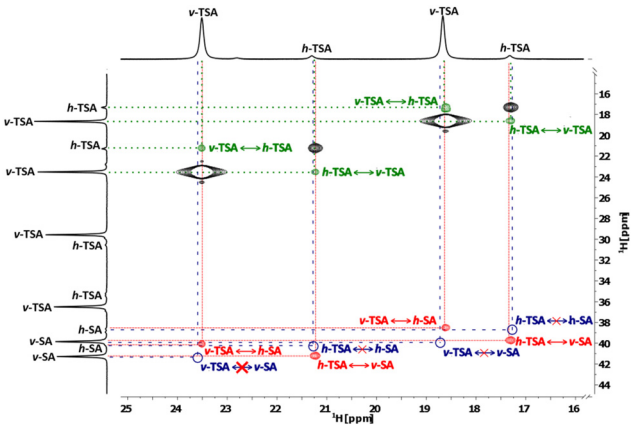


**Fig. 6** A part of the $^1$H–$^1$H EXSY spectrum of the [Eu(do3ap$^{Me}$)]$^-$ complex at 5 °C and $\tau_m$ = 15 ms (600 MHz) showing cross-peaks between signals of axial protons corresponding to processes not inverting macrocycle conformation: red – pendant arms re-orientation, green – phosphonate rotation. The empty blue circles show positions of hypothetical cross-peaks for a combined phosphinate rotation and pendant arms re-orientation. The diagonal peaks are black.

as averages at multiple mixing times (Table S7), and their values were checked by comparison of values of equilibrium constants calculated from these rate constants and from the $^{31}$P signal intensities (Table S8). To compare rates of the processes, values weighted by the isomer abundances were used (Table 2).

The rate of macrocycle inversion for the [Eu(do3ap$^{Me}$)]$^-$ complex is approximately the same as for the Eu$^{III}$ complexes of other $H_4$dota derivatives, consistent with the fact that macrocycle inversion is generally independent of the pendant arms substitution.[73,74] However, the pendant arms re-orientation is slower than the macrocycle inversion in the [Eu(do3ap$^{Me}$)]$^-$ complex while it is faster in the complexes of derivatives with phosphonate groups or carboxamide pendant arms.[37,38,75,76] Rate of pendant arms re-orientation is generally very sensitive to the pendant arms substitution, being the fastest for complexes with carboxamide pendant arms like DOTAM and slowed down with an increase in pendant arms bulkiness. Substitution on α-carbon atoms of pendant arm acetates completely halts the process. The pendant arms re-orientation rate in the [Eu(do3ap$^{Me}$)]$^-$ anion is the slowest among the complexes with non-α-substituted acetates which is likely caused by the steric requirements of the tetrahedral methyl group (if compared with an oxygen atom, *e.g.*, in the phosphonate monoesters) and/or by different electronic effects of the electron-donating methyl group if compared with electron-withdrawing OH/OEt groups. This effect is likely similar to the decrease of pendant arms re-orientation rate by substituting the amine on carboxamide pendant arms, as seen by the drastic difference in the process rates between DOTAM and DTMA.[75,76]

## Phosphinate rotation

The $^1$H–$^1$H EXSY confirmed the phosphinate rotation interchanging *v*-TSA and *h*-TSA. Previously, two possible mecha-

**Table 2** Weighted averages of rate constants (5 °C) for dynamic processes in $Eu^{III}$ complexes of $H_4do3ap^{Me}$ and analogous ligands (ligand structures are shown in Fig. 1). Charges of the species are omitted

| | | Rate constant $k$ [$s^{-1}$] for the [Eu(**L**)] complexes of the ligands | | | | | | |
|---|---|---|---|---|---|---|---|---|
| Exchanging isomers | Process[a] | $do3ap^{Me}$ | $do3ap^{OEt}$ | Hdo3ap/do3ap[b] | dota | dotam[c] | dtma[c] | dotmam[c] |
| *h*-TSA/*h*-SA | Cycle | 17.1 | 11.4 [37] | 21.2/17.8[d] [38] | 17.8[d] [38] | —[e] [75] | 23[d] [76] | 41[d] [76] |
| *v*-TSA/*v*-SA | Cycle | 13.3 | 10.6 [37] | | | | | |
| *h*-TSA/*v*-SA | Arms | 1.73 | 32.4 [37] | 24/83.3[d] [38] | 9.1[d] [38] | 592[d] [75] | 172[d] [76] | —[e] [76] |
| *v*-TSA/*h*-SA | Arms | 7.41 | 11.4 [37] | | | | | |
| *h*-TSA/*v*-TSA | Phos | 2.54 | 6.4 [37] | —[f] | —[f] | —[f] | —[f] | —[f] |

[a] Process abbreviations: cycle = macrocycle inversion, arms = pendant arms re-orientation and phos = phosphinate/phosphonate rotation. [b] Data for monoprotonated (**L** = Hdo3ap) and deprotonated (**L** = do3ap, as dianion) complexes. [c] Rate constants were calculated from the published activation parameters. [d] Only one SA and one TSA isomer are present in these complexes containing non-chiral/no phosphorus atom. [e] The process is very slow. [f] Not applicable to this systems.

nisms not involving a decoordination of the phosphorus acid group were proposed:[37] (i) Phosphorus group rotation changing only the phosphorus atom configuration, *i.e.*, *v*-TSA/*h*-TSA or *v*-SA/*h*-SA interchange, and (ii) a simultaneous phosphorus group rotation and pendant arms re-orientation, *i.e.*, *h*-TSA/*h*-SA or *v*-TSA/*v*-SA interchange. Based on the presence of cross-peaks between the *v*-TSA/*h*-TSA axial protons and the lack of the *h*-TSA/*h*-SA or *v*-TSA/*v*-SA axial protons cross-peaks in the $^1H$–$^1H$ EXSY spectrum of the $Eu^{III}$ complex (Fig. 4), the mechanism of phosphinate rotation is the same as that of phosphonate rotation, *i.e.*, proceeding through a simple rotation of the phosphinate group changing the phosphorus atom configuration but preserving the pendant arms orientation.

Furthermore, this mechanism was confirmed combining DFT calculations and variable-temperature (VT) $^{17}O$ NMR (Table S4, Fig. S18 and S19). In principle, up to eight signals are observable by $^{17}O$ NMR for the title complexes (signals of the coordinated and non-coordinated oxygen atoms of four diastereoisomers) but signals of different diastereoisomers are often indistinguishable due to mutual overlap. At low temperatures, signals of coordinated and non-coordinated oxygen atoms were well separated for all paramagnetic complexes. Signals of non-coordinated oxygen atoms, but not those of coordinated oxygen atoms, could be detected even for the $Gd^{III}$ complex, analogously to the $Gd^{III}$ complexes of $H_4$dota and $H_4do3ap^{OEt}$.[22,37] Usually, NMR signals are undetectable for $Gd^{III}$ complexes due to the fast relaxation, with $^{17}O$ NMR signals of non-coordinated oxygen atoms being the notable exception.[22,37] With temperature increase, signals of coordinated oxygen atoms of different diastereoisomers coalesce first, and the same applies to signals of non-coordinated oxygens of different diastereoisomers. Then, the coordinated and non-coordinated phosphinate oxygen atoms, each represented by a coalesced signal consisting of up to four signals of different diastereoisomers, interchange with an increase in signal linewidths. These processes are detectable for complexes of $Ln^{III}$ ions larger than $Gd^{III}$. Thus, the variable-temperature (VT) $^{17}O$ NMR spectra were evaluated as an interchange between two equally populated sites, as the oxygen atoms of the same type (coordinated or non-coordinated) but originating from different diastereoisomers of the studied $Ln^{III}$ (La–Sm) complexes coalesce at a lower temperature than the lowest experimental temperature. The determined rate constants (Table S9) were used to calculate activation parameters with the Eyring equation (Table 3, Table S10 and Fig. S20). The

**Table 3** Free energies of activation and the corresponding rate constants for the *h*-TSA/*v*-TSA phosphinate/phosphonate rotations determined from VT $^{17}O$ NMR and by DFT calculations for the $[Ln(do3ap^{Me})]^-$ and $[Ln(do3ap^{OEt})]^-$ complexes. Free energies of activation for theoretical *h*-SA/*v*-SA and *h*-TSA′/*v*-TSA′ phosphinate rotations predicted by DFT are also shown

| | $[Ln(do3ap^{Me})]^{-}$[a] | | | | $[Ln(do3ap^{OEt})]^{-}$[b] | |
|---|---|---|---|---|---|---|
| $Ln^{III}$ | $^{298}\Delta G^{\ddagger}$ [kJ $mol^{-1}$] | $^{298}\Delta G^{\ddagger}_{calc}$ (TSA) [kJ $mol^{-1}$] | $k_{obs}$ (5 °C) [$s^{-1}$] | $^{298}\Delta G^{\ddagger}_{calc}$ (SA)[c] [kJ $mol^{-1}$] | $^{298}\Delta G^{\ddagger}$ [kJ $mol^{-1}$] | $^{298}G^{\ddagger}_{calc}$ [kJ $mol^{-1}$] |
| La | 57.7 | 28.8 | $2.52 \times 10^5$ | 37.8 | 51.8 | 52/36.0[a] |
| Ce | 50.9 | 31.9 | $1.60 \times 10^3$ | 41.2 | 52.9 | 55.6 |
| Pr | 54.3 | 37.4 | $3.68 \times 10^2$ | 45.6 | 55.7 | 58 |
| Nd | 56 | 42.7 | $1.77 \times 10^2$ | 49.7 | 57.1 | 61.2 |
| Sm | 63.5 | 49.6 | 6.89 | 58.3 | 64 | 69 |
| Eu | —[d] | 52.9 | 2.54[e] | 62.7 | 61 | 71.5/59.7[a] |
| Yb | —[f] | 107.8 (TSA′)[g] | —[f] | — | —[f] | —[h] |

[a] This work. [b] Values from the literature (ref. 37). [c] Values for hypothetical *h*-SA/*v*-SA exchange. [d] It could not be determined due to the influence of TSA/SA exchange processes. [e] Value from 2D $^{31}P$–$^{31}P$ EXSY. [f] Exchange was not detected experimentally. [g] Value for hypothetical *h*-TSA′/*v*-TSA′ exchange. [h] Not calculated.

 

$^{298}\Delta G^{\ddagger}$ values for the phosphinate rotation have the same magnitude as that for the phosphonate rotation,[37] pendant arms re-orientation and the macrocycle inversion[38,74–83] in $Ln^{III}$ complexes of $H_4$dota and its amide or phosphonate derivatives but they are much lower than those for the carboxylate rotation (Table S11).[19,21] Activation energies increase with decreasing $Ln^{III}$ ion size, and the trend is similar for the phosphonate, phosphinate and carboxylate rotations (Fig. 7).[19,21,37]

Here, the activation energies of pendant arms re-orientation and the macrocycle inversion in complexes of large $Ln^{III}$ ions follow the same trend as in complexes of $H_4$dota-like ligands, and are similar to those for the phosphinate rotation in the $H_4$do3ap$^{Me}$ complexes (Table S11).[74,81] These trends are usually caused by an increase in charge density for the smaller $Ln^{III}$ ions but are much more profound for the phosphinate, phosphonate and carboxylate rotations due to steric effects. The $Ln^{III}$ ions are localised progressively deeper in the ligand cavity with the decreasing ion size,[24,64] making their transition states with the $\kappa^2$-$PO_2$/$\kappa^2$-$CO_2$ bidentate binding progressively less favourable. While the phosphonate rotation was detected in [Ln(do3ap$^{OEt}$)]$^-$ complexes for La–Tb, the phosphinate rotation was observed in [Ln(do3ap$^{Me}$)]$^-$ complexes only for La–Eu (Table 3). The phosphinate rotation is also slower in the [Eu(do3ap$^{Me}$)]$^-$ complex than in the [Eu(do3ap$^{OEt}$)]$^-$ anion based on $^1$H–$^1$H EXSY data (Table 2). This is likely due to the same steric effect as the decrease in the rate of pendant arms re-orientation if comparing re-orientation in the [Eu(do3ap$^{OEt}$)]$^-$ complex and that in other $Eu^{III}$ complexes (see above). The comparison also indicates that the *P*-methyl group with a "branched" $-CH_3$ group is bulkier than the phosphonate group(s) where the first phosphorus-bound atom is a "non-branched" oxygen atom. However, the activation free energies of both rotations are nearly the same in complexes of $La^{III}$–$Sm^{III}$ ions. Thus, the steric effect of the phosphorus substituent seems to affect the processes only if the $Ln^{III}$ ion is localised deeper in the ligand cavity.

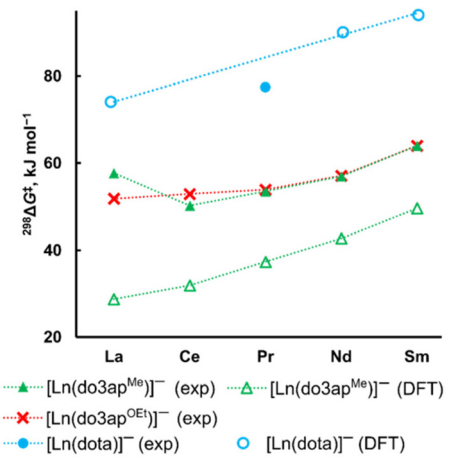


**Fig. 7** Activation free energies $^{298}\Delta G$ determined by VT $^{17}$O NMR or DFT for phosphinate/phosphonate rotation in the [Ln(do3ap$^{Me/OEt}$)]$^-$ complexes and for carboxylate rotation in [Ln(dota)]$^-$. Data for the complexes of $H_4$dota and $H_4$do3ap$^{OEt}$ were taken from literature.[19,21,37] Lines are included only as guides for the eyes.

The phosphinate rotation was confirmed by DFT calculations. Relative energies of all diastereoisomers of complexes of large $Ln^{III}$ ions and of the $Yb^{III}$ ion, energies of the corresponding transition states for the exchanges between *h*-SA/*v*-SA and *h*-TSA/*v*-TSA were calculated (Table S4). The calculated activation Gibbs energies for the *v*-TSA/*h*-TSA exchange are shown in Fig. 7 and Table 3, and they agree with the trend in experimental values determined from VT $^{17}$O NMR, but are somewhat lower. This is likely due to the difficulties of modelling solvent effects by DFT using polarized continuum models. In particular, our calculations appear to over-stabilize the transition state responsible for the *v*-TSA/*h*-TSA exchange, which displays a bidentate $\kappa^2$-$PO_2$ coordination. This group is probably forming rather strong hydrogen bonds with water molecules in solution. These directional interactions are not well described by PCM,[84] resulting in an overestimation of the interaction between the metal ion and the bidentate $\kappa^2$-$PO_2$ group. These limitations of PCM were evidenced previously while investigating the rotation of acetate groups in DOTA derivatives.[19]

The theoretical activation energies for the *v*-SA/*h*-SA exchange are higher than those for the *v*-TSA/*h*-TSA exchange for all $Ln^{III}$ ions. This, together with the absence of cross-peaks corresponding to this exchange in $^1$H-$^1$H EXSY spectrum of the $Eu^{III}$ complex, shows that the *v*-SA and *h*-SA isomers do not interconvert by phosphinate rotation. The same behaviour was observed for the phosphonate rotation in the [Ln(do3ap$^{OEt}$)]$^-$ complexes.[37] Based on the experimental data, the phosphinate rotation was also not detected for the "anhydrous" *v*-TSA′/*h*-TSA′ isomers, in line with the very large theoretical value of $^{298}G^{\ddagger}_{calc}$ = 107.8 kJ mol$^{-1}$ calculated for this process. Thus, the phosphinate rotation was confirmed only in the TSA diastereoisomers of the [Ln(do3ap$^{Me}$)]$^-$ complexes for Ln = La–Eu. The phosphinate rotation proceeds by a mechanism analogous to that of the phosphonate rotation, and both exchange processes have similar rates.

In the complexes investigated here, all isomers are in a dynamic equilibrium and pure isomers cannot be present in solution. Thus, properties of an individual isomer cannot be directly determined. However, even a small abundance of one isomer can influence the macroscopic properties of such complexes in solution. A classical example of this behaviour is the different water exchange dynamics of the SA and TSA isomers of DOTA derivatives which influences their properties as MRI CA's.[16,75,76] For the *vertical*/*horizontal* isomers, the structures of the first coordination sphere are very similar each other, according to the X-ray data, but differences in the second hydration sphere may be expected. This is relevant for the design of MRI CAs. Thus, we performed DFT calculations with one coordinated and four second-sphere water molecules for all four isomers of the [Gd($H_2O$)(do3ap$^{Me}$)]$^-$ complex. The calculations showed (Fig. S21) that the second-sphere water molecules are more ordered in both *horizontal* isomers. The $Gd^{III}$ coordinated water distance, Gd–$O_w$, is similar in both SA isomers (2.583 and 2.617 Å for *v*-SA and *h*-SA, respectively) but

significantly different in the TSA isomers (2.718 and 2.629 Å for *v*-TSA and *h*-TSA, respectively). Thus, the *v*-TSA isomer might exchange the coordinated water molecule significantly faster than the other isomers. On the other hand, the more ordered second-sphere hydration in the *horizontal* isomers might influence the bulk water relaxation or fluorescence quenching more than that in *vertical* isomers. To test these hypotheses, complexes with a defined configurationally stable arrangement on phosphorus atom(s) have to be prepared. This can be, in principle, achieved with optically active phosphine oxide pendant arm(s), or perhaps by locking a given configuration of the complex by ligand C-functionalization.[85]

## Conclusions

In this work, we introduced a new method for the determination of the absolute configuration on a chiral tetrahedral phosphorus atom in solution. The method is suitable for rigid systems and a paramagnetic metal has to be used as probe/label. A combination of DFT calculations and $^{13}C$ PRE allows identification of the location of the substituents on the phosphorus atom. Here, the defined spatial arrangement was assured by a coordination of the phosphorus group to a metal ion. In general, the method can be used for other (semi)rigid complexes/systems where the Ln···X distances in solution are fixed and the necessary NMR data can be obtained in a presence of the paramagnetic probe located at a close distance to alter the relaxation times of the measured nucleus. In principle, the method might be used in systems with any paramagnetic $Ln^{III}$ ion as a probe and for atoms of any non-quadrupolar NMR-active nuclei.

The lanthanide(III) complexes of the title ligand, $H_4$do3ap$^{Me}$, can be present as four diastereoisomers. All expected diastereoisomers *v*-TSA, *h*-TSA, *v*-SA and *h*-SA were identified, but with a low abundance of the minor diastereoisomers, *h*-TSA and *h*-SA. The method presented here enables us to assign the observed NMR signals to the *vertical*/*horizontal* diastereoisomers for complexes of this type for the first time. Thus, they were experimentally attributed by determining the distances between the $Yb^{III}$ ion and the *P*-bound methyl $^{13}C$ atoms in the [Yb(do3ap$^{Me}$)]$^-$ complex from NMR data. These distances were compared with those obtained by DFT calculations and X-ray diffraction data. Through comparison with previously published data, the orientation of a phosphorus substituent in complexes of other phosphorus acid $H_4$dota analogues was also assigned.

Isomerism and dynamics of $Ln^{III}$ complexes of $H_4$do3ap$^{Me}$, were investigated by multinuclear NMR and DFT calculations. The diastereoisomers are in mutual exchange, observable by NMR. The interchange of the diastereoisomers was confirmed by $^1H$–$^1H$ EXSY experiments and proceeds by the expected processes, *i.e.*, pendant arms re-orientation, macrocycle inversion and phosphinate rotation. The phosphinate rotation is fully analogous to the recently reported phosphonate rotation, but it was confirmed for a phosphinate group for the first time here. The phosphinate and phosphonate rotations proceed by analogous mechanisms through an intermediate with bidentate $\kappa^2$-$PO_2$ coordination. Based on VT NMR and DFT calculations, the phosphinate rotation occurs only in complexes of large $Ln^{III}$ ions ($La^{III}$–$Eu^{III}$) and only in diastereoisomers with TSA geometry, analogously to the monophosphonate complexes. The data point to somewhat higher bulkiness of the P–$CH_3$ moiety compared with a phosphonate monoester fragment, P–O–R. Thus, on the basis of our data, a prediction on isomer preferences in complexes of macrocyclic ligands is now possible. For instance, in complexes of phosphinate $H_4$dota derivatives, the very bulky phosphorus substituent should induce an exclusive preference for the *vertical* isomers.

These findings contribute to further elucidation of the solution isomerism/dynamics of $Ln^{III}$ complexes of phosphorus acid derivatives of $H_4$dota, which will help in the design of new complexes for specific applications. The position of the phosphorus substituent subtly alters the arrangement of the ligand in the complexes, which could be employed in the design of $Ln^{III}$ complexes with tailored properties.

The scope of "a phosphorus group rotation" was confirmed to be wider than just in phosphonate complexes and seems to be a general feature, expected to take place even in coordinated phosphates in biochemistry. Thus, the methods presented here may be applied to areas across the chemistry of phosphorus acid derivatives.

## Experimental

The general experimental methods, synthesis of the unlabelled $H_4$do3ap$^{Me}$, the $^{17}O$-labelled ethyl methylphosphinate and the $H_4$do3ap$^{Me}$ complexes, and experimental information for the X-ray crystal structure determination are in the Experimental Details section of the SI. The NMR spectra of all complexes were measured in $D_2O$ at pD ~6.5 adjusted by diluted LiOD/$D_2O$ or DCl/$D_2O$ solutions at 14.1 T (*i.e.* at 600 MHz for $^1H$).

### Synthesis of $^{17}O$-labelled $H_4$do3ap$^{Me}$

The $^{17}O$-labelled (approx. 12% enrichment on each phosphinate oxygen atom) title ligand was prepared following Scheme 1 from the *t*$Bu_3$do3a·HBr and $^{17}O$-labelled ethyl methyl-*H*-phosphinate which was prepared from methyldichlorophosphine and $^{17}O$-enriched water (see SI).

### Compound 4

The *t*$Bu_3$do3a·HBr **1** (4.87 g, 8.2 mmol) was dissolved in anhydrous pyridine (40 ml). The freshly prepared solution of ethyl methyl-*H*-phosphinate (7.3 mmol) in $CH_2Cl_2$ (20 ml) and paraformaldehyde (0.90 g, 30 mmol) were added to this mixture. The mixture was stirred at 40 °C for 36 h. The volatiles were evaporated from the reaction mixture *in vacuo*. The residue was partially dissolved in $CH_2Cl_2$ (100 ml) and washed with 20% (w/w) aq. $K_2CO_3$ (100 ml) and water (100 ml). The organic phase was dried with $Na_2SO_4$, the drying agent was filtered off on a glass frit and washed with $CH_2Cl_2$ (approx. 50 ml). After evapor-

 

ation of volatiles from the filtrate at reduced pressure, the mixture of compound **4** (approx. 50 molar%), *t*Bu$_3$do3a and a by-product, *N*-methylated *t*Bu$_3$do3a, was obtained. This mixture was used in the subsequent reaction without further purification. $^{31}$P NMR (162 MHz, $CDCl_3$) $\delta$: 52.5–52.9 (m). $^{17}$O NMR (54 MHz, $CDCl_3$) $\delta$: 97 (bs, 1O, $CH_2P(O)(CH_3)\underline{O}Et$), 101 (bs, 1O, $CH_2P(\underline{O})(CH_3)(OEt)$). MS (ESI$^+$): $m/z$ = 635.7 [M($^{16}$O) + H]$^+$, 636.5 [M($^{17}$O) + H]$^+$. TLC (EtOH–conc. aq. $NH_3$ 20 : 1): $R_f$ = 0.7.

### $^{17}$O-labelled $H_4$do3ap$^{Me}$

The mixture containing compound **4** from the previous step was dissolved in anhydrous $CHCl_3$ (~200 ml), and excess TMSBr (12 ml, 91 mmol) was slowly added. The mixture was stirred at room temperature in the dark for 72 h, and volatiles were evaporated *in vacuo*. The residue was dissolved in $CH_3OH$ (~200 ml), the solution was stirred for 1 h, and volatiles were evaporated *in vacuo*. The residue was dissolved in a $CH_2Cl_2$–TFA mixture (1 : 1, 200 ml) and the solution was stirred at room temperature for 2 d. Volatiles were evaporated at reduced pressure, and the residual TFA was co-evaporated with $CH_3OH$ (50 ml) *in vacuo*. The residue was dissolved in a minimal amount of water, and the solution was passed through an Amberlite CG50 weak cation exchange resin ($H^+$-cycle, 6 × 4 cm, the resin was washed with approx. 400 ml of water). Volatiles from the eluate were evaporated *in vacuo*, the residue was re-dissolved in a minimal amount of water, and further purified on a Dowex-50 W×4 strong cation-exchange resin ($H^+$-cycle, 5 × 40 cm). The resin was washed with water until the eluate pH was neutral. The product was eluted with 10% aq. pyridine (approx. 400 ml). Volatiles were evaporated at reduced pressure. The residue was dissolved in a minimal amount of water and further purified by chromatography on Amberlite CG50 weak cation exchanger ($H^+$-cycle, 5 × 40 cm, elution by water). Volatiles were evaporated from the combined product-containing fractions. The residue was dissolved in MeOH (approx. 10 ml) with a few drops of water, and the product was precipitated by a slow addition of EtOH (approx. 30 ml) followed by a slow addition of $Et_2O$ (approx. 30 ml). The precipitate was filtered on a fine glass frit, washed with $Et_2O$ (3 × 30 ml) and dried in an oven (90 °C, 15 min). The product was isolated as a white powder comprised of the zwitter-ionic ($^{17}$O)$H_4$do3ap$^{Me}$·2$H_2O$ (0.7 g, 17% based on Me-$PCl_2$, ~12% $^{17}$O at each oxygen atom of the phosphinate group). $^{17}$O NMR (54 MHz, $D_2O$/CsOD, 85 °C, pD ≈ 14) $\delta$: 121 (d, $^1J_{OP}$ 109 Hz). MS (ESI$^+$): $m/z$ 439.3 [M($^{16}$O) + H]$^+$, 440.4 [M($^{17}$O) + H]$^+$, 461.3 [M($^{16}$O) + Na]$^+$, 462.3 [M($^{17}$O) + Na]$^+$. The $^1$H, $^{13}$C and $^{31}$P NMR spectra and TLC data are the same as those of the non-labelled $H_4$do3ap$^{Me}$ (see SI).

### Determination of $^{13}$C NMR relaxation times

The $^{13}$C $T_{1,2}$ NMR relaxation times of the paramagnetic [Yb(do3ap$^{Me}$)]$^-$ complex were determined at 5 °C (see SI), where dynamic processes are slow and have negligible effects on the relaxation rates. Paramagnetic $T_{1,M}$ and $T_{2,M}$ were calculated from these values by subtracting the $T_1$ and $T_2$ values for the analogous signals in the diamagnetic [Lu(do3ap$^{Me}$)]$^-$ complex determined by the same methods. Differences in paramagnetic relaxation times were used to determine the Yb–$^{13}$C distances in the complex. First, value of the rotational correlation time $\tau_R$ was determined from $^{13}$C $T_1$ values and NOE factors of the $CH_2$ signals of a diamagnetic complex; the same approximation was successfully used for complexes of $H_4$dota before.[86] The NOE factor was determined by comparing the signal intensities in two $^{13}$C NMR experiments, one with and one without $^1$H NOE, measured by the standard pulse-acquire sequence with relaxation delay of $d_1 \sim 10T_1$. Then, the $\tau_R$ was approximated by eqn (1) and (2) where $R_1$ is the $^{13}$C longitudinal relaxation rate, $R_1^{DD}$ is the dipolar $^{13}$C longitudinal relaxation rate, NOE is the NOE enhancement factor, $r_{CH}$ is the $CH_2$ carbon–proton distance taken as 1.09 Å based on the DFT-optimized structure, $N_H$ is the number of hydrogen atoms bonded to the carbon atom, $\gamma_H = 2.675 \times 10^8/\gamma_C = 6.728 \times 10^8$ rad s$^{-1}$ T$^{-1}$ are the $^1$H and $^{13}$C magnetogyric ratios, respectively, and $\hbar = 1.0546 \times 10^{-34}$ J s is the reduced Planck constant.

$$R_1^{DD} = R_1 \frac{NOE}{1.988} \quad (1)$$

$$\tau_R = \frac{R_1^{DD} r_{CH}^6}{N_H \gamma_H{}^2 \gamma_C{}^2 \hbar^2} \quad (2)$$

In this way, the value of rotational correlation time, $\tau_R \sim 138$ ps, was determined from $^{13}$C NMR relaxation times of the pendant arm and macrocycle $CH_2$ groups of the diamagnetic [Lu(do3ap$^{Me}$)]$^-$ complex (Table S2). This rotational correlation time was used to determine Yb–C distance using Yb$^{III}$ as a paramagnetic probe. Paramagnetic enhancements of longitudinal $T_{1,M}$ and transverse $T_{2,M}$ relaxation times of NMR signals of nuclei in Ln$^{III}$ complexes consist of contact $T_{i,c}$, dipolar $T_{i,p}$ and Curie $T_{i,\chi}$ ($i$ = 1,2) contributions.[61] The contact contribution, $T_{i,c}$, is usually negligible for Ln ≠ Gd and for nuclei not directly bound to the Ln$^{III}$ ion. The dipolar and Curie contributions, $T_{i,p}$ and $T_{i,\chi}$, were separated as dipolar relaxation times $T_{1,p}$ and $T_{2,p}$ are very similar for Ln ≠ Gd. Thus, the Curie contribution of the Yb$^{III}$ complex atoms not directly bound to Yb$^{III}$ could be separated from the difference between $T_{1,M}$ and $T_{2,M}$.[54] This difference depends only on the distance of the nucleus from the Yb$^{III}$ ion and on the rotational correlation time $\tau_R$ of the complex. Thus, $^{13}$C NMR PRE of the *P*-methyl group could be used for the phosphorus atom configuration assignment. The $^{13}$C NMR relaxation times used for the determination of Yb–C distances in the [Yb(do3ap$^{Me}$)]$^-$ complex were determined at 5 °C where dynamic processes are slow and have negligible effects on the NMR relaxation times. The Yb–C distances $r$ were then computed from the difference of the paramagnetic $T_{1,M}$ and $T_{2,M}$ relaxation times of the particular $^{13}$C nuclei as defined by eqn (3).[61]

$$\frac{1}{T_{2,M}} - \frac{1}{T_{1,M}} = \frac{1}{5}\left(\frac{\mu_0}{4\pi}\right)^2 \frac{\gamma_C{}^2 \mu_{eff}{}^4 H_0{}^2}{(3kT)^2 r^6}\left(4\tau_R - \frac{3\tau_R}{1+\omega_C{}^2\tau_R{}^2}\right) \quad (3)$$

Here, $(\mu_0/4\pi) = 10^{-7}$ N A$^{-2}$ is the magnetic permeability of vacuum, $\gamma_C$ is the $^{13}$C magnetogyric ratio (see above), $\mu_{eff} = 4.173 \times 10^{-23}$ J T$^{-1}$ is the effective magnetic moment

of $Yb^{III}$, $H_0$ [in $T$] is the external magnetic field strength, $k = 1.381 \times 10^{-23}$ J $K^{-1}$ is the Boltzmann constant, $T$ is the thermodynamic temperature, $\omega_C$ is the Larmor frequency of $^{13}C$ and $\tau_R$ is the rotational correlation time of the complex.

To determine the $H_3\underline{C}\cdots Yb$ distance, the ratio of paramagnetically enhanced $R_{1M}$ relaxation rates of the carbonyl and methyl carbon atoms at 0 and 5 °C can also be used. Here, the $Yb\cdots{}^{13}C$ distance is the only parameter that changes values of $R_{1M}$ for different $^{13}C$ sites. Then, the $H_3\underline{C}\cdots Yb$ distance can be calculated according to eqn (4)[61] where $d_X$ are distances of the nuclei and $R_{1M,X}$ are the corresponding transverse relaxation rates.

$$\frac{d_A}{d_B} = \sqrt[6]{\frac{R_{1M,B}}{R_{1M,A}}} \quad (4)$$

### Quantitative EXSY spectra

The 2D $^{31}P$ EXSY was used to determine the rate constants of dynamic processes. Integral intensities of all $^{31}P$ EXSY signals were determined by signal deconvolution in Topspin© after phase and baseline corrections. Rate constants and relaxation times of signals were calculated at each mixing time $\tau_m$ in Matlab© by the eqn (5)[87,88] describing a dependence between rate constants and integral intensities of the signals. Here, **R** is a 4 × 4 matrix containing the rate constants of all dynamic processes and $R_1$ relaxation rates of signals of all four diastereoisomers, and **A** is a 4 × 4 matrix containing integral intensities of signals divided by initial integral intensities $I_0$ (for definition of **R** and **A**, see SI).

$$\mathbf{R} = -\frac{\ln(\mathbf{A})}{\tau_m} \quad (5)$$

Initial integral intensities $I_0$ were interpolated from the $^{31}P$ EXSY spectra measured at short mixing times ($\tau_m$ = 0.001, 0.01 and 0.1 s). After the calculation, outliers (defined as three scaled median absolute deviations from the median) were removed from the calculated parameters, and the rate constants and relaxation times were calculated as the mean of the remaining values.

### DFT calculations

All calculations in this work were performed in ORCA 6.0[89] using DFT with the wB97X functional and Grimme's D4 dispersion correction.[90–92] All calculations were performed with a large integration grid (DEFGRID3),[93] a tight SCF energy convergence threshold and RIJCOSX approximation.[94–96] Geometry optimizations for all diastereoisomers and transition states of the $[Ln(do3ap^{Me/OEt/H/tBu})]^-$ complexes were performed employing the large core effective core potentials of the Stuttgart type for all $Ln^{III}$,[97] ECP(46 + $n$)MWB which include 46 + $4f^n$ electrons in the core, with the corresponding (6s6p5d)/[4s4p4d] + 2s1p1d basis sets for the valence space. For all remaining atoms, the def2tzvp basis set was used.[98,99] For transition states, the Hessian was calculated before the geometric optimisation and then after each five steps. For complexes of large $Ln^{III}$ (La–Eu), models with one coordinated water molecule were used. For complexes of smaller $Yb^{III}$, no explicit water molecule was used. Bulk solvent effects of water were accounted for by the conductor-like polarisation continuum model.[100] To study the second coordination sphere in $Gd^{III}$ complexes, models with one coordinated and four more explicit water molecules were used. All optimised structures were tested by the frequency analysis at the same computational level. Relative free energies (zero-point energies and thermal terms at 25 °C) were also obtained by frequency analysis.

### Variable-temperature NMR

The VT NMR data were processed in Mestrenova© where phase and baseline were corrected. Diastereoisomer ratios were determined from the signals integrated or deconvoluted to a Lorentzian–Gaussian shape (for overlapping signals). Kinetic parameters of the oxygen atom exchange were determined from these pre-processed spectra in Asymexfit[101] as the best fit to the analytical solution of Bloch-McConnel equations, analogously to the approach used previously for the phosphonate rotation[37] (for details, see SI). Activation parameters, $\Delta H^‡$, $\Delta S^‡$ and $\Delta G^‡$, of the phosphinate rotation were determined by fitting the temperature dependence of the rate constants to the Eyring law, eqn (6) and (7). Here, $k_B$, $h$ and $R$ are the Boltzmann, Planck and universal gas constant, respectively. The $\Delta H^‡$ and $\Delta S^‡$ were considered temperature-independent.

$$k = \frac{k_B T}{h} \exp\left(-\frac{\Delta H^‡}{RT}\right) \exp\left(\frac{\Delta S^‡}{R}\right) \quad (6)$$

$$\Delta G^‡ = \Delta H^‡ - T\Delta S^‡ \quad (7)$$

## Author contributions

A. S. – syntheses of ligands and complexes, NMR measurements, DFT calculations, study concept; J. K. – X-ray data fitting, C. P. I. – DFT calculations, supervision of DFT calculations; P. H. – study concept and money acquisition. All authors participated in the manuscript writing.

## Conflicts of interest

There are no conflicts to declare.

## Data availability

The data supporting this article have been included as part of the supplementary information (SI). Supplementary information: details on synthesis of ligands and complexes; X-ray experimental data and extended discussion of solid-state structures; $^1H$, $^{17}O$ and $^{31}P$ NMR spectra of $Ln^{III}$ complexes; NMR relaxation rate of selected nuclei in complexes; various 2D

 

NMR spectra of complexes; DFT-calculated energies and structures of complexes; abundances of isomeric species for complexes of different $Ln^{III}$ ions; $^{17}O$ VT-NMR spectra; experimental values of rate constants and activation parameters; definition of matrixes and equations used for calculations. See DOI: https://doi.org/10.1039/d5qi01885d.

CCDC 2470192–2470194 contain the supplementary crystallographic data for this paper.[102a–c]

## Acknowledgements

We thank Dr I. Císařová for X-ray data collection and Dr Z. Tošner for help with NMR measurements. The work was supported by GACR (22-34083S) and the Grant Agency of Charles University (no. 68122 to A. S.). Computational resources were provided by CESGA – Centro de Supercomputación de Galicia (C. P. I. and A. S.) and the e-INFRA CZ project (ID: 90254), supported by the Ministry of Education, Youth and Sports of the Czech Republic.

## References

1 J. Wahsner, E. M. Gale, A. Rodríguez-Rodríguez and P. Caravan, Chemistry of MRI contrast agents: Current challenges and new frontiers, *Chem. Rev.*, 2019, **119**, 957–1057.
2 H. Li and T. J. Meade, Molecular magnetic resonance imaging with Gd(III)-based contrast agents: Challenges and key advances, *J. Am. Chem. Soc.*, 2019, **141**, 17025–17041.
3 P. Caravan, J. J. Ellison, T. J. McMurry and R. B. Lauffer, Gadolinium(III) chelates as MRI contrast agents: structure, dynamics, and applications, *Chem. Rev.*, 1999, **99**, 2293–2352.
4 P. Hermann, J. Kotek, V. Kubíček and I. Lukeš, Gadolinium(III) complexes as MRI contrast agents: Ligand design and properties of the complexes, *Dalton Trans.*, 2008, 3027–3047.
5 R. E. Mewis and S. J. Archibald, Biomedical applications of macrocyclic ligand complexes, *Coord. Chem. Rev.*, 2010, **254**, 1686–1712.
6 M. C. Heffern, L. M. Matosziuk and T. J. Meade, Lanthanide probes for bioresponsive imaging, *Chem. Rev.*, 2014, **114**, 4496–4539.
7 C. S. Cutler, H. M. Hennkens, N. Sisay, S. Huclier-Markai and S. S. Jurisson, Radiometals for combined imaging and therapy, *Chem. Rev.*, 2013, **113**, 858–883.
8 E. W. Price and C. Orvig, Matching chelators to radiometals for radiopharmaceuticals, *Chem. Soc. Rev.*, 2014, **43**, 260–290.
9 T. I. Kostelnik and C. Orvig, Radioactive main group and rare earth metals for imaging and therapy, *Chem. Rev.*, 2019, **119**, 902–956.
10 E. Mathieu, A. Sipos, E. Demeyere, D. Phipps, D. Sakaveli and K. E. Borbas, Lanthanide-based tools for the investigation of cellular environments, *Chem. Commun.*, 2018, **54**, 10021–10035.
11 U. Cho and J. K. Chen, Lanthanide-based optical probes of biological systems, *Cell Chem. Biol.*, 2020, **27**, 921–936.
12 D. Parker, J. D. Fradgley and K. L. Wong, The design of responsive luminescent lanthanide probes and sensors, *Chem. Soc. Rev.*, 2021, **50**, 8193–8213.
13 E. Ravera, L. Gigli, L. Fiorucci, C. Luchinat and G. Parigi, The evolution of paramagnetic NMR as a tool in structural biology, *Phys. Chem. Chem. Phys.*, 2022, **24**, 17397–17416.
14 Q. Miao, C. Nitsche, H. Orton, M. Overhand, G. Otting and M. Ubbink, Paramagnetic chemical probes for studying biological macromolecules, *Chem. Rev.*, 2022, **122**, 9571–9642.
15 D. Joss and D. Häussinger, Design and applications of lanthanide chelating tags for pseudocontact shift NMR spectroscopy with biomacromolecules, *Prog. NMR Spectrosc.*, 2019, **114–115**, 284–312.
16 J. A. Peters, K. Djanashvili, C. F. G. C. Geraldes and C. Platas-iglesias, Structure, dynamics, and computational studies of lanthanide-based contrast agents, in *The Chemistry of Contrast Agents in Medical Magnetic Resonance Imaging*, Wiley, Chichester, 2nd edn, 2013, pp. 209–276.
17 S. Aime, M. Botta, M. Fasano, M. P. M. Marques, C. F. G. C. Geraldes, D. Pubanz and A. E. Merbach, Conformational and coordination equilibria on DOTA Complexes of lanthanide metal ions in aqueous solution studied by $^{1}H$-NMR spectroscopy, *Inorg. Chem.*, 1997, **36**, 2059–2068.
18 C. Platas-Iglesias, The solution structure and dynamics of MRI probes based on lanthanide(III) DOTA as investigated by DFT and NMR spectroscopy, *Eur. J. Inorg. Chem.*, 2012, 2023–2033.
19 F. Mayer, C. Platas-Iglesias, L. Helm, J. A. Peters and K. Djanashvili, $^{17}O$ NMR and density functional theory study of the dynamics of the carboxylate groups in DOTA complexes of lanthanides in aqueous solution, *Inorg. Chem.*, 2012, **51**, 170–178.
20 L. Fusaro and M. Luhmer, $^{17}O$ NMR study of diamagnetic and paramagnetic lanthanide(III)-DOTA complexes in aqueous solution, *Inorg. Chem.*, 2014, **53**, 8717–8722.
21 L. Fusaro and M. Luhmer, An oxygen-17 dynamic NMR study of the Pr-DOTA complex, *Dalton Trans.*, 2014, **43**, 967–972.
22 L. Fusaro, G. Casella and A. Bagno, Direct detection of $^{17}O$ in $[Gd(DOTA)]^{-}$ by NMR spectroscopy, *Chem. – Eur. J.*, 2015, **21**, 1955–1960.
23 J. Rudovský, P. Cígler, J. Kotek, P. Hermann, P. Vojtíšek, I. Lukeš, J. A. Peters, L. Vander Elst and R. N. Muller, Lanthanide(III) complexes of a mono(methylphosphonate) analogue of $H_4$dota: The influence of protonation of the phosphonate moiety on the TSAP/SAP isomer ratio and the water exchange rate, *Chem. – Eur. J.*, 2005, **11**, 2373–2384.

24 P. Vojtíšek, P. Cígler, J. Kotek, J. Rudovský, P. Hermann and I. Lukeš, Crystal structures of lanthanide(III) complexes with cyclen derivative bearing three acetate and one methylphosphonate pendants, *Inorg. Chem.*, 2005, **44**, 5591–5599.

25 J. Rudovský, J. Kotek, P. Hermann, I. Lukeš, V. Mainero and S. Aime, Synthesis of a bifunctional monophosphinic acid DOTA analogue ligand and its lanthanide(III) complexes. A gadolinium(III) complex endowed with an optimal water exchange rate for MRI applications, *Org. Biomol. Chem.*, 2005, **3**, 112–117.

26 P. Lebdušková, P. Hermann, L. Helm, É. Tóth, J. Kotek, K. Binnemans, J. Rudovský, I. Lukeš and A. E. Merbach, Gadolinium(III) complexes of mono- and diethyl esters of monophosphonic acid analogue of DOTA as potential MRI contrast agents: Solution structures and relaxometric studies, *Dalton Trans.*, 2007, 493–501.

27 P. Urbanovský, J. Kotek, F. Carniato, M. Botta and P. Hermann, Lanthanide complexes of DO3A-(dibenzylamino)methylphosphinate: Effect of protonation of the dibenzylamino group on the water-exchange rate and the binding of human serum albumin, *Inorg. Chem.*, 2019, **58**, 5196–5210.

28 M. Purgel, Z. Baranyai, A. de Blas, T. Rodríguez-Blas, I. Bányai, C. Platas-Iglesias and I. Tóth, An NMR and DFT investigation on the conformational properties of lanthanide(III) 1,4,7,10-tetraazacyclododecane-1,4,7,10-tetraacetate analogues containing methylenephosphonate pendant arms, *Inorg. Chem.*, 2010, **49**, 4370–4382.

29 C. F. G. C. Geraldes, A. D. Sherry and G. E. Kiefer, The solution structure of $Ln(DOTP)^{5-}$ complexes. A comparison of lanthanide-induced paramagnetic shifts with the MMX energy-minimized structure, *J. Magn. Reson.*, 1992, **97**, 290–304.

30 F. Avecilla, J. A. Peters and C. F. G. C. Geraldes, Crystal structure of a sodium salt of $[Gd(DOTP)]^{5-}$: Implications for Its second-sphere relaxivity and the $^{23}Na$ NMR hyperfine shift effects of $[Tm(DOTP)]^{5-}$, *Eur. J. Inorg. Chem.*, 2003, 4179–4186.

31 S. Aime, A. S. Batsanov, M. Botta, J. A. K. Howard, D. Parker, K. Senanayake and G. Williams, Solution and solid-state characterization of highly rigid, eight-coordinate lanthanide(III) complexes of a macrocyclic tetrabenzylphosphinate, *Inorg. Chem.*, 1994, **33**, 4696–4706.

32 S. Aime, A. S. Batsanov, M. Botta, R. S. Dickins, S. Faulkner, C. E. Foster, A. Harrison, J. a. K. Howard, J. M. Moloney, T. J. Norman, D. Parker and J. A. G. Williams, Nuclear magnetic resonance, luminescence and structural studies of lanthanide complexes with octadentate macrocyclic ligands bearing benzylphosphinate groups, *J. Chem. Soc., Dalton Trans.*, 1997, 3623–3636.

33 J. Rohovec, P. Vojtíšek, P. Hermann, J. Mosinger, Z. Žák and I. Lukeš, Synthesis, crystal structures and NMR and luminescence spectra of lanthanide complexes of 1,4,7,10-tetraazacyclododecane with *N*-methylene(phenyl)phosphinic acid pendant arms, *J. Chem. Soc., Dalton Trans.*, 1999, 3585–3592.

34 W. D. Kim, G. E. Kiefer, J. Huskens and A. D. Sherry, NMR studies of the lanthanide(III) complexes of 1,4,7,10-tetraazacyclododecane-1,4,7,10-tetrakis[methanephospho-nic acid mono(2,2′,2′-trifluoroethyl) ester], *Inorg. Chem.*, 2002, **36**, 4128–4134.

35 Z. Kotková, G. A. Pereira, K. Djanashvili, J. Kotek, J. Rudovský, P. Hermann, L. Vander Elst, R. N. Muller, C. F. G. C. Geraldes, I. Lukeš and J. A. Peters, Lanthanide (III) complexes of phosphorus acid analogues of $H_4$DOTA as model compounds for the evaluation of the second-sphere hydration, *Eur. J. Inorg. Chem.*, 2009, 119–136.

36 G. A. Pereira, L. Ball, A. D. Sherry, J. A. Peters and C. F. G. C. Geraldes, NMR characterization of lanthanide (3+) complexes of tetraazatetrakisphosphinato and tetraazatetrakis phosphonato ligands, *Helv. Chim. Acta*, 2009, **92**, 2532–2551.

37 A. Svítok, J. Blahut, P. Urbanovský and P. Hermann, Dynamics of coordinated phosphonate group directly observed by $^{17}O$–NMR in lanthanide(III) complexes of a mono(ethyl phosphonate) DOTA analogue, *Chem. – Eur. J.*, 2024, **30**, e202400970.

38 J. Blahut, P. Hermann, Z. Tošner and C. Platas-Iglesias, A combined NMR and DFT study of conformational dynamics in lanthanide complexes of macrocyclic DOTA-like ligands, *Phys. Chem. Chem. Phys.*, 2017, **19**, 26662–26671.

39 S. C. L. Kamerlin, P. K. Sharma, R. B. Prasad and A. Warshel, Why nature really chose phosphate, *Q. Rev. Biophys.*, 2013, **46**, 1–132.

40 J.-B. Wang, J. Y. Lv, S. K. Bankar, S.-S. Fang and M. Shang, Stereoselective synthesis of *P*-stereogenic nucleotide prodrugs and oligonucleotides, *Chem. Soc. Rev.*, 2025, **54**, 9370–9406.

41 C. Nowlan, Y. Li, J. C. Hermann, T. Evans, J. Carpenter, E. Ghanem, B. K. Shoichet and F. M. Raushel, Resolution of chiral phosphate, phosphonate, and phosphinate esters by an enantioselective enzyme library, *J. Am. Chem. Soc.*, 2006, **128**, 15892–15902.

42 P.-C. Tsai, Y. Fan, J. Kim, L. Yang, S. C. Almo, Y. Q. Gao and F. M. Raushel, Structural determinants for the stereoselective hydrolysis of chiral substrates by phosphotriesterase, *Biochemistry*, 2010, **49**, 7988–7997.

43 C. Boehme and G. Wipff, The energetic and structural effects of steric crowding in phosphate and dithiophosphinate complexes of lanthanide cations $M^{3+}$: A computational study, *Chem. – Eur. J.*, 2001, **7**, 1398–1407.

44 E. Mayaan, K. Range and D. M. York, Structure and binding of Mg(II) ions and di-metal bridge complexes with biological phosphates and phosphoranes, *J. Biol. Inorg. Chem.*, 2004, **9**, 807–817.

45 E. L. Christian, V. E. Anderson, P. R. Carey and M. E. Harris, A quantitative Raman spectroscopic signal for metal-phosphodiester interactions in solution, *Biochemistry*, 2010, **49**, 2869–2879.

 

46 A. S. Petrov, J. Funseth-Smotzer and G. R. Pack, Computational study of dimethyl phosphate anion and its complexes with water, magnesium, and calcium, *Int. J. Quantum Chem.*, 2005, **102**, 645–655.
47 K. Moedritzer and R. R. Irani, Aminomethylphosphonic acids, Mannich-type reactions with orthophosphorous acid, *J. Org. Chem.*, 1966, **31**, 1603–1607.
48 V. Theodorou, K. Skobridis, D. Alivertis and I. P. Gerothanassis, Synthetic methodologies in organic chemistry involving incorporation of [$^{17}$O] and [$^{18}$O] isotopes, *J. Labelled Compnd. Radiopharm.*, 2014, **57**, 481–508.
49 J. Zhang, E. Lambert, Z. F. Xu, J. Brioche, P. Remy and S. R. Piettre, From oxygen to sulfur and back: Difluoro-*H*-phosphinothioates as a turning point in the preparation of difluorinated phosphinates: Application to the synthesis of modified dinucleotides, *J. Org. Chem.*, 2019, **84**, 5245–5260.
50 K. M. Błazewska, McKenna reaction - Which oxygen attacks bromotrimethylsilane?, *J. Org. Chem.*, 2014, **79**, 408–412.
51 S. Aime, M. Botta, D. Parker and J. A. G. Williams, Nuclear magnetic resonance studies of neutral lanthanide(III) complexes with tetraaza-macrocyclic ligands containing three phosphinate and one carboxamide co-ordinating arms, *J. Chem. Soc., Dalton Trans.*, 1995, 2259–2266.
52 S. Aime, M. Botta, R. S. Dickins, C. L. Maupin, D. Parker, J. P. Riehl and J. A. G. Williams, Synthesis, NMR, relaxometry and circularly polarised luminescence studies of macrocyclic monoamide-tris(phosphinate) complexes bearing a remote chiral centre, *J. Chem. Soc., Dalton Trans.*, 1998, 881–892.
53 K. Momma and F. Izumi, VESTA 3 for three-dimensional visualization of crystal, volumetric and morphology data, *J. Appl. Crystallogr.*, 2011, **44**, 1272–1276.
54 S. Aime, L. Barbero, M. Botta and G. Ermondi, Determination of metal-proton distances and electronic relaxation times in lanthanide complexes by nuclear magnetic resonance spectroscopy, *J. Chem. Soc., Dalton Trans.*, 1992, 225–228.
55 M. D. C. Fernández-Fernández, R. Bastida, A. Macías, P. Pérez-Lourido, C. Platas-Iglesias and L. Valencia, Lanthanide(III) complexes with a tetrapyridine pendant-armed macrocyclic ligand: $^{1}$H NMR structural determination in solution, X-ray diffraction, and density-functional theory calculations, *Inorg. Chem.*, 2006, **45**, 4484–4496.
56 S. Koeller, G. Bernardinelli, B. Bocquet and C. Piguet, A novel extended covalent tripod for assembling nine-coordinate lanthanide(III) podates: A delicate balance between flexibility and rigidity, *Chem. – Eur. J.*, 2003, **9**, 1062–1074.
57 L. Brachais and M. Visseaux, NMR $T_1$-relaxation measurements on paramagnetic organolanthanides: An alternative tool for structure determination in solution, *Eur. J. Inorg. Chem.*, 2005, 2486–2492.
58 J. W. Walton, R. Carr, N. H. Evans, A. M. Funk, A. M. Kenwright, D. Parker, D. S. Yufit, M. Botta, S. D. Pinto and K. L. Wong, Isostructural series of nine-coordinate chiral lanthanide complexes based on triazacyclononane, *Inorg. Chem.*, 2012, **51**, 8042–8056.
59 K. H. Chalmers, E. De Luca, N. H. M. Hogg, A. M. Kenwright, I. Kuprov, D. Parker, M. Botta, J. I. Wilson and A. M. Blamire, Design principles and theory of paramagnetic fluorine-labelled lanthanide complexes as probes for $^{19}$F magnetic resonance: A proof-of-concept study, *Chem. – Eur. J.*, 2010, **16**, 134–148.
60 J. Rudovský, M. Botta, P. Hermann, A. Koridze and S. Aime, Relaxometric and solution NMR structural studies on ditopic lanthanide(III) complexes of a phosphinate analogue of DOTA with a fast rate of water exchange, *Dalton Trans.*, 2006, 2323–2333.
61 J. A. Peters, J. Huskens and D. J. Raber, Lanthanide induced shifts and relaxation rate enhancements, *Prog. NMR Spectrosc.*, 1996, **28**, 283–350.
62 J. A. Peters, K. Djanashvili, C. F. G. C. Geraldes and C. Platas-Iglesias, The chemical consequences of the gradual decrease of the ionic radius along the Ln-series, *Coord. Chem. Rev.*, 2020, **406**, 213146.
63 I. Lukeš, J. Kotek, P. Vojtíšek and P. Hermann, Complexes of tetraazacycles bearing methylphosphinic/phosphonic acid pendant arms with copper(II), zinc(II) and lanthanides(III). A comparison with their acetic acid analogues, *Coord. Chem. Rev.*, 2001, **216–217**, 287–312.
64 P. Urbanovský, J. Kotek, I. Císařová and P. Hermann, The solid-state structures and ligand cavity evaluation of lanthanide(III) complexes of a DOTA analogue with a (dibenzylamino)methylphosphinate pendant arm, *Dalton Trans.*, 2020, **49**, 1555–1569.
65 J. Kotek, J. Rudovský, P. Hermann and I. Lukeš, Three in one: TSA, TSA′, and SA units in one crystal structure of a yttrium(III) complex with a monophosphinated $H_4$dota analogue, *Inorg. Chem.*, 2006, **45**, 3097–3102.
66 T. Vitha, V. Kubíček, J. Kotek, P. Hermann, L. Vander Elst, R. N. Muller, I. Luke and J. A. Peters, Gd(III) complex of a monophosphinate-bis(phosphonate) DOTA analogue with a high relaxivity; Lanthanide(III) complexes for imaging and radiotherapy of calcified tissues, *Dalton Trans.*, 2009, 3204–3214.
67 K. P. Pulukkody, T. J. Norman, D. Parker, L. Royle and C. J. Broan, Synthesis of charged and uncharged complexes of gadolinium and yttrium with cyclic polyazaphosphinic acid ligands for in vivo applications, *J. Chem. Soc., Perkin Trans. 2*, 1993, 605–620.
68 S. Procházková, V. Kubíček, J. Kotek, A. Vágner, J. Notni and P. Hermann, Lanthanide(III) complexes of monophosphinate/monophosphonate DOTA-analogues: Effects of the substituents on the formation rate and radiolabelling yield, *Dalton Trans.*, 2018, **47**, 13006–13015.
69 E. Cole, R. C. B. Copley, J. A. K. Howard, D. Parker, G. Ferguson, J. F. Gallagher, B. Kaitner, A. Harrison and L. Royle, 1,4,7-Triazacyclononane-1,4,7-triyl-trimethylene-tris(phenylphosphinate) enforces octahedral geometry: Crystal and solution structures of its metal complexes and

comparative biodistribution studies of radiolabelled indium and gallium complexes, *J. Chem. Soc., Dalton Trans.*, 1994, 1619–1629.

70 J. Notni, P. Hermann, J. Havlíčková, J. Kotek, V. Kubíček, J. Plutnar, N. Loktionova, P. J. Riss, F. Rösch and I. Lukeš, A triazacyclononane-based bifunctional phosphinate ligand for the preparation of multimeric $^{68}$Ga tracers for positron emission tomography, *Chem. – Eur. J.*, 2010, **16**, 7174–7185.

71 J. Šimeček, M. Schulz, J. Notni, J. Plutnar, V. Kubíček, J. Havlíčková and P. Hermann, Complexation of metal ions with TRAP (1,4,7-triazacyclononane phosphinic acid) ligands and 1,4,7-triazacyclononane-1,4,7-triacetic acid: Phosphinate-containing ligands as unique chelators for trivalent gallium, *Inorg. Chem.*, 2012, **51**, 577–590.

72 S. Hoeft and K. Roth, Struktur und dynamik von lanthanoid–tetraazacyclododecantetraacetat–(DOTA–) komplexen in lösung, *Chem. Ber.*, 1993, **126**, 869–873.

73 D. Parker, R. S. Dickins, H. Puschmann, C. Crossland and J. A. K. Howard, Being excited by lanthanide coordination complexes : Aqua species, chirality, excited-state chemistry, and exchange dynamics, *Chem. Rev.*, 2010, **102**, 1977–2010.

74 E. N. Zapolotsky, Y. Qu and S. P. Babailov, Lanthanide complexes with polyaminopolycarboxylates as prospective NMR/MRI diagnostic probes: peculiarities of molecular structure, dynamics and paramagnetic properties, *J. Inclusion Phenom. Macrocyclic Chem.*, 2022, **102**, 1–33.

75 F. A. Dunand, S. Aime and A. E. Merbach, First $^{17}$O NMR observation of coordinated water on both isomers of [Eu(DOTAM)$(H_2O)]^{3+}$: A direct access to water exchange and its role in the isomerization, *J. Am. Chem. Soc.*, 2000, **122**, 1506–1512.

76 F. A. Dunand, R. S. Dickins, D. Parker and A. E. Merbach, Towards rational design of fast water-exchanging Gd(dota-like) contrast agents? Importance of the M/m ratio, *Chem. – Eur. J.*, 2001, **7**, 5160–5167.

77 J. F. Desreux, Nuclear magnetic resonance spectroscopy of lanthanide complexes with a tetraacetic tetraaza macrocycle, Unusual conformation properties, *Inorg. Chem.*, 1980, **19**, 1319–1324.

78 S. P. Babailov, E. N. Zapolotsky, A. I. Kruppa, P. A. Stabnikov, I. A. Godovikov, E. v. Bocharov and E. S. Fomin, Two types of conformational dynamics and thermo-sensor properties of praseodymium-DOTA by $^{1}$H/$^{13}$C NMR, *Inorg. Chim. Acta*, 2019, **486**, 340–344.

79 Q. Miao, R. Dekkers, K. B. S. S. Gupta, M. Overhand, R. Dasgupta and M. Ubbink, Rigidified and hydrophilic DOTA-like lanthanoid ligands: Design, synthesis, and dynamic properties, *Inorg. Chem.*, 2023, **62**, 3776–3787.

80 S. P. Babailov, P. v. Dubovskii and E. N. Zapolotsky, Paramagnetic lanthanides as magnetic resonance thermosensors and probes of molecular dynamics: Holmium-DOTA complex, *Polyhedron*, 2014, **79**, 277–283.

81 S. P. Babailov and E. N. Zapolotsky, Tm-DOTA as responsive relaxation and shift probe for NMR local temperature monitoring at high magnetic fields, *Inorg. Chim. Acta*, 2021, **517**, 120153.

82 V. Jacques and J. F. Desreux, Quantitative two-dimensional EXSY spectroscopy and dynamic behavior of a paramagnetic lanthanide macrocyclic chelate: YbDOTA (DOTA = 1,4,7,10-tetraazacyclododecane-*N*,*N*′,*N*″,*N*‴-tetraacetic acid), *Inorg. Chem.*, 1994, **33**, 4048–4053.

83 S. Aime, A. Barge, M. Botta, M. Fasano, J. D. Ayala and G. Bombieri, Crystal structure and solution dynamics of the lutetium(III) chelate of DOTA, *Inorg. Chim. Acta*, 1996, **246**, 423–429.

84 V. S. Bryantsev, M. S. Diallo and W. A. Goddard III, Calculation of solvation free energies of charged solutes using mixed cluster/continuum models, *J. Phys. Chem. B*, 2008, **112**, 9709–9719.

85 J. Zhang, L. Dai, L. He, A. Bhattarai, C.-M. Chan, W. C.-S. Tai, V. Vardhanabhuti and G.-L. Law, Design and synthesis of chiral DOTA-based MRI contrast agents with remarkable relaxivities, *Commun. Chem.*, 2023, **6**, 251.

86 S. Aime, M. Botta and G. Ermondi, An NMR relaxation study of aqueous solutions of Gd(III) chelates, *J. Magn. Reson.*, 1991, **92**, 572–580.

87 C. L. Perrin and T. J. Dwyer, Application of two-dimensional NMR to kinetics of chemical exchange, *Chem. Rev.*, 1990, **90**, 935–967.

88 Z. Zolnai, N. Juranić, D. Vikić-Topić and S. Macura, Quantitative determination of magnetization exchange rate constants from a series of two-dimensional exchange NMR spectra, *J. Chem. Inf. Comput. Model.*, 2000, **40**, 611–621.

89 F. Neese, Software update: The ORCA program system – Version 6.0, *Wiley Interdiscip. Rev.: Comput. Mol. Sci.*, 2025, **15**, e70019.

90 E. Caldeweyher, J. M. Mewes, S. Ehlert and S. Grimme, Extension and evaluation of the D4 London-dispersion model for periodic systems, *Phys. Chem. Chem. Phys.*, 2020, **22**, 8499–8512.

91 E. Caldeweyher, C. Bannwarth and S. Grimme, Extension of the D3 dispersion coefficient model, *J. Chem. Phys.*, 2017, **147**, 034112.

92 E. Caldeweyher, S. Ehlert, A. Hansen, H. Neugebauer, S. Spicher, C. Bannwarth and S. Grimme, A generally applicable atomic-charge dependent London dispersion correction, *J. Chem. Phys.*, 2019, **150**, 154122.

93 F. Neese, The SHARK integral generation and digestion system, *J. Comput. Chem.*, 2023, **44**, 381–396.

94 F. Neese, An improvement of the resolution of the identity approximation for the formation of the Coulomb matrix, *J. Comput. Chem.*, 2003, **24**, 1740–1747.

95 F. Neese, F. Wennmohs, A. Hansen and U. Becker, Efficient, approximate and parallel Hartree–Fock and hybrid DFT calculations. A 'chain-of-spheres' algorithm for the Hartree–Fock exchange, *Chem. Phys.*, 2009, **356**, 98–109.

96 D. Bykov, T. Petrenko, R. Izsák, S. Kossmann, U. Becker, E. Valeev and F. Neese, Efficient implementation of the

 

analytic second derivatives of Hartree–Fock and hybrid DFT energies: a detailed analysis of different approximations, *Mol. Phys.*, 2015, **113**, 1961–1977.

97 M. Dolg, H. Stoll, A. Savin and H. Preuss, Energy-adjusted pseudopotentials for the rare earth elements, *Theor. Chim. Acta*, 1989, **75**, 173–194.

98 F. Weigend, Accurate Coulomb-fitting basis sets for H to Rn, *Phys. Chem. Chem. Phys.*, 2006, **8**, 1057–1065.

99 G. L. Stoychev, A. A. Auer and F. Neese, Automatic generation of auxiliary basis sets, *J. Chem. Theory Comput.*, 2017, **13**, 554–562.

100 M. Garcia-Ratés and F. Neese, Efficient implementation of the analytical second derivatives of Hartree–Fock and hybrid DFT energies within the framework of the conductor-like polarizable continuum model, *J. Comput. Chem.*, 2019, **40**, 1816–1828.

101 V. Římal, H. Štěpánková and J. Štěpánek, Analysis of NMR spectra in case of temperature-dependent chemical exchange between two unequally populated sites, *Concepts Magn. Reson., Part A*, 2011, **38A**, 117–127.

102 (*a*) CCDC 2470192: Experimental Crystal Structure Determination, 2025, DOI: **10.5517/ccdc.csd.cc2nxfmn**; (*b*) CCDC 2470193: Experimental Crystal Structure Determination, 2025, DOI: **10.5517/ccdc.csd.cc2nxfnp**; (*c*) CCDC 2470194: Experimental Crystal Structure Determination, 2025, DOI: **10.5517/ccdc.csd.cc2nxfpq**.